3

Electroencephalography and High-Density Electrophysiological Source Localization

DIEGO A. PIZZAGALLI

1. INTRODUCTION

In 1924, Hans Berger, a German psychiatrist, performed the first electroencephalographic (EEG) recording in humans (Berger, 1929), a discovery that was initially greeted with great skepticism by the scientific community. By recording from one electrode placed over the forehead and one over the occipital cortex, Berger discovered the existence of rhythmic activity oscillating at approximately 10 Hz, particularly during relaxed wakefulness and in the absence of sensory stimulation or mental activity. In this landmark discovery, Berger described for the first time what would become known as alpha waves. As a result, Berger was among the first to suggest that the periodic fluctuations of the human EEG may be associated with mental processes, including arousal, memory, and consciousness. Over the years, developments in data collection and analyses transformed EEG into one of the prime techniques for studying the human brain. Table 3.1 summarizes selected landmark discoveries and developments that have contributed shaping the EEG field throughout the century.

The past two decades in particular have witnessed unparalleled progress in our ability to image human brain function noninvasively. Different imaging techniques are currently available to investigate brain function based on hemodynamic (functional magnetic resonance imaging, fMRI), metabolic (positron emission tomography, PET), or electromagnetic (electroencephalography, EEG; magnetoencephalography, MEG) measurements. In order to investigate spatiotemporal dynamics of brain activity, methods that directly assess neural activity are required. By measuring electrical activity of neuronal assemblies with millisecond temporal resolution, EEG and MEG, unlike hemodynamic techniques, offer the possibility of studying brain function in real time. Unfortunately, as will be discussed in this chapter, the spatial resolution afforded by EEG/MEG is constrained by several factors. The most important of these factors are the distorting effects of the head volume conductor,[1] low signal-to-noise

[1] Volume conduction refers to the process of current flow from the electrical generator to the recording electrode (Fisch, 1999).

ratios, and limited spatial sampling due to practical limits on the numbers of electrodes that can be utilized. More importantly, it soon became evident that the neuroelectromagnetic "inverse problem" (the attempt to identify generating sources of measured, scalp-recorded EEG signals) is fundamentally ill-posed. As first described in 1853 by Helmholtz, there are an infinite number of source configurations that can explain a given set of scalp-recorded potentials. Thus, at a first glance, the quest for the development of methods combining millisecond temporal resolution with millimeter spatial resolution appears to be a lost cause. Fortunately, solutions to the inverse problem can be found by postulating physiologically and anatomically sound assumptions about putative EEG sources and by mathematically implementing established laws of electrodynamics.

The main purpose of the present chapter is to review recent advances in the EEG field (event-related potentials, ERPs, will not be discussed here, as they are reviewed elsewhere in this volume.) To understand these developments it will first be necessary to detail the physiological basis of the EEG signal. Subsequently, important issues associated with data acquisition, signal processing, and quantitative analyses will be discussed (see Davidson, Jackson, & Larson, 2000; Pivik et al., 1993; Gasser & Molinari, 1996; Nunez et al., 1997; Nuwer et al., 1999; Thakor & Tong, 2004 for more comprehensive reviews of these topics). The largest portion of the chapter will be devoted to reviewing emerging source localization techniques that have been shown to localize EEG activity without postulating a priori assumptions about the number of underlying sources (Baillet et al., 2001; Michel et al., 2004). As we will discuss, perhaps the greatest advancements in the EEG field in the last 5–10 years have been achieved in the development of these localization techniques, in particular when used in concert with high-density EEG recording, realistic head models, and other functional neuroimaging techniques. The picture emerging in light of these achievements reveals that the spatial resolution of the EEG may be substantially higher than previously thought, thus opening exciting and new opportunities for investigating spatiotemporal

Table 3.1. Selected historical landmarks in electroencephalography (adapted from Maurer & Dierks, 1991 and Neidermeyer, 1993)

Year	Name	Description
1875	R. Caton	First tracing in animals of fluctuating potentials that constitute the EEG
1924	H. Berger	First human EEG measurement
1929	H. Berger	First human EEG publication in *Archive für Psychiatrie und Nervenheilkunde*
1932	J. T. Toennies	First ink-writing biological amplifier
1932	G. Dietch	First application of Fourier analyses on human EEG
1934	F. Gibbs	First systematic application of the EEG to epilepsy
1935	A. L. Loomins	First systematic application of the EEG to sleep
1936	W. G. Walter	Discovery of slow (delta) activity in the presence of tumors
1942	K. Motokawa	First EEG brain map
1943	I. Bertrand and R. S. Lacape	First book on EEG modeling
1947		American EEG Society is founded
1947	G. D. Dawson	First demonstration of human evoked potential responses
1949		*Electroencepahlography and Clinical Neurophysiology,* the first EEG journal, is launched
1952	A. Remond and F. A. Offner	First topographic analyses of occipital EEG
1952	M. A. B. Brazier and J. U. Casby	Introduction of auto- and cross-correlation function
1955	A. Remond	Application of topographical EEG analyses
1958	H. Jasper	Introduction of 10–20 system for standardized electrode placement
1960	W. R. Adley	Introduction of Fast Fourier Transformation (start of computerized spectral analyses)
1961	T. M. Itil	Application of EEG analyses for classification of psychopharmacological agents
1963	N. P. Bechtereva	Localization of focal brain lesions by EEG
1965	J. W. Cooley and J. W. Tukey	Introduction of fast Fourier algorithm
1968	D. O. Walter	Introduction of coherence analyses for the human EEG
1970	B. Hjorth	Development of new quantitative methods, including source derivation
1971	D. Lehmann	First multichannel topography of human alpha EEG fields
1973	M. Matousek and I. Petersen	Development of age-corrected EEG spectral parameter for detecting pathology (qEEG)
1977	E. R. John	Introduction of "neurometrics" (standardized qEEG analyses with normative databases)
1978	R. A. Ragot and A. Remond	EEG field mapping
1979	F. H. Duffy	Introduction of brain electrical activity mapping (BEAM)

dynamics of brain mechanisms underlying mental processes and dysfunctions in psychopathology, bringing us closer to fulfillment of Berger's dream that EEG will open a "window to the mind."

2. PHYSIOLOGICAL BASIS OF THE EEG

2.1. EEG generation: I. The role of post-synaptic potentials in cortical pyramidal neurons

In the central nervous system, when a neuron is activated by other neurons through afferent action potentials, excitatory post-synaptic potentials (EPSPs) are triggered at its apical dendrites. When this occurs, the membrane of the apical dendrites becomes depolarized and electronegative, compared to the cell soma (Baillet et al., 2001; Speckmann, Elger, & Altrup, 1993). As a consequence of this transient potential difference, current flows from the nonexcited soma to the excited apical dendritic tree, and a negative polarity emerges at the surface (Speckmann et al., 1993).[2] In the opposite case, with excitation of the soma, the current flow will have inverse direction.

[2] Negative potentials at the surface can arise either due to (a) superficial EPSPs (i.e., excitation at apical dendrites) or (b) deep IPSPs (i.e., inhibition of the soma). Conversely, positive potentials at the surface can arise either due to (a) superficial IPSPs (i.e., inhibition at apical dendrites) or (b) deep EPSPs (i.e., excitation of the soma; Speckmann et al., 1993).
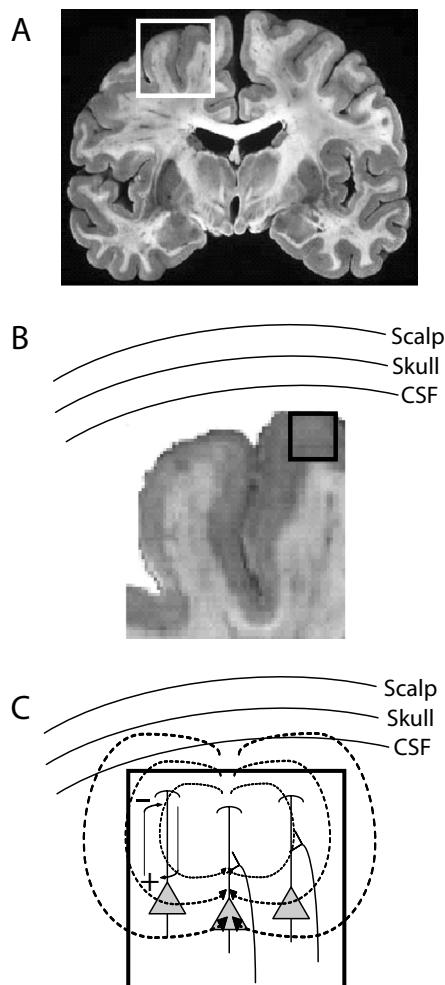
Figure 3.1. Neurophysiological basis of EEG generation. Scalp-recorded EEG oscillations generated by summation of excitatory and inhibitory post-synaptic potentials in cortical pyramidal neurons. (A) A coronal slice of the human brain is shown, with cortical gray matter highlighted in grey color. (B) An expanded view of cerebral gyri and sulci (see inset in A) is shown in relations to the scalp, skull, and cerebral spinal fluid (CSF). (C) A schematic illustration of cortical pyramidal cells within the cortical mantle (see inset in B) is shown. In this example, an excitatory post-synaptic potential (EPSP) is generated at the cell soma; local excitation (+ and −) leads to a tangential current flow (solid lines). The closed loops (dashed lines) represent the summation of extracellular currents produced by the postsynaptic potentials at cortical pyramidal cells, whose dendritic trunks are parallel to each others and perpendicular to the cortical surface. The deep EPSP shown in the example would produce a positive field potentials at the cortical surface (Speckmann et al., 1993).

Scalp-recorded EEG oscillations are hypothesized to be generated by the summation of excitatory and inhibitory post-synaptic potentials in cortical pyramidal neurons (Speckmann et al., 1993; Figure 3.1). In the generation of an EEG oscillation, tens of thousands of synchronously activated pyramidal cortical neurons are assumed to be involved. The coherent orientation of their dendritic trunks (parallel to each others and perpendicular to the cortical surface) allows summation and propagation to the scalp surface (Nunez & Silberstein, 2000). Accordingly, although subcortical contributions to scalp-recorded EEG have been reported (e.g., Llinas, Ribary, Jeanmonod, Kronberg, & Mitra, 1999), cortical macrocolums are thought to be the main contributors of EEG signals (Fisch, 1999; Baillet et al., 2001).

2.2. EEG generation: II. The role of thalamo-cortical networks

Although mechanisms underlying EEG generation are not fully understood, interactions between thalamic and cortical networks are assumed to play a key role in various rhythmical EEG activities (Steriade, 1993). In animals, neurophysiological evidence has shown that several thalamic, thalamocortical, and cortical neurons display intrinsic oscillatory patterns, which in turn generate rhythmic EEG oscillations. The thalamus, in particular, has been described as a key player in the generation of alpha and beta oscillations. Accordingly, thalamic oscillations in the 7.5–12.5 Hz frequency range have been shown to activate the firing of cortical neurons (Steriade, 1993). The associated depolarization, which mainly occurs in the cortical layer IV, in turn creates a dipolar source with negativity in layer IV and positivity in superficial layers. Placing electrodes at the scalp allows measurement of small but reliable far-field potentials representing the summation of these potential fluctuations. In humans, thalamic contributions to alpha oscillations were investigated in a study integrating positron emission tomography (PET) and EEG recordings (Larson et al., 1998). Cortical alpha power was found to be inversely correlated to glucose metabolism in the thalamus, consistent with the assumption that thalamic activity in response to sensory or cortical input may lead to alpha suppression.

Corticocortical and thalamocortical interactions during information processing have also been postulated in the generation of oscillations at higher frequencies, including the beta band (13–30 Hz). Notably, the thalamus has been also implicated in the generation of delta waves (1–4 Hz), which might arise through interactions between deep cortical layers and the thalamus that are normally inhibited by afferents from the ascending reticular activating system. In addition, the septohippocampal system and various limbic regions (e.g., hippocampus, cingulate cortex) have been implicated in the generation of theta oscillations (Vinogradova, 1995; Bland & Oddie, 1998).

In sum, EEG oscillations appear to be dependent on interactions between the cortex and the thalamus, which both produce intrinsically rhythmical activities. Whereas the thalamus has been critically implicated in the pacing of such rhythmical activities, the cortex provides the coherent output in response to thalamic input and generates the vast majority of oscillations that can be recorded at the scalp (Fisch, 1999).

2.3. EEG generation: III. The role of local-scale and large-scale synchronization

As mentioned above, at any given moment in time, the signal recorded at the scalp is due to spatial summation of current density induced by synchronized post-synaptic potential occurring in large clusters of neurons. Considering that the diameter of EEG electrodes ($\sim$10 mm) is several orders of magnitude larger than single neurons ($\sim$20 μm) and that the area of an electrode covers approximately 250,000 neurons (Baillet et al., 2001), it is clear that many neurons must be activated synchronously in order to detect an EEG signal at the scalp.

Consistent with this notion, animal studies have described substantial synchronization among neighboring neurons ("local-scale synchronization"; e.g., Llinas, 1988), as well as between neuronal assemblies of distant brain regions ("large-scale synchronization"; e.g., Bressler & Kelso, 2001). Thus, synchronization of oscillations is a key mechanism for neuronal communication between spatially distributed brain networks (see Schnitzler & Gross, 2005 for a recent review). Emerging animal evidence indicates that oscillatory processes might (a) bias input selection, (b) temporally bind neurons into assemblies, and (c) foster synaptic plasticity (Buzsaki & Draguhn, 2004). Intriguingly, higher frequency oscillations (e.g., gamma) appear to originate from smaller neuronal assemblies, whereas low frequency oscillations (e.g., theta) span larger neuronal populations (Buzsaki & Draguhn, 2004). Large-scale neuronal synchronization plays an important role in various cognitive processes that rely on distributed neuronal networks (e.g., language processing; Weiss & Mueller, 2003), and can be studied through EEG coherence analysis, as will be discussed further in Section 5.3.

3. NORMATIVE EEG ACTIVITY

The millisecond temporal resolution of EEG allows scientists to investigate not only fluctuations of EEG activity (i.e., increases/decreases) as a function of task demand or subject samples but also to differentiate between functional inhibitory and excitatory activities. As a general rule, low frequencies (e.g., delta and theta) show large synchronized amplitudes, whereas high EEG frequencies (e.g., beta and gamma) show small amplitude due to high degree of desynchronization in the underlying neuronal activity. In adults, the amplitude of normative EEG oscillations lies between 10 and 100 μV (more commonly between 10 and 50 μV; Niedermeyer, 1993). In the following section, a brief review of various EEG bands and their putative functional roles will be presented. For a review of the molecular and physiological basis underlying the generation of various EEG oscillations, the interested reader is referred to Steriade (1993) and Speckmann et al. (1993).
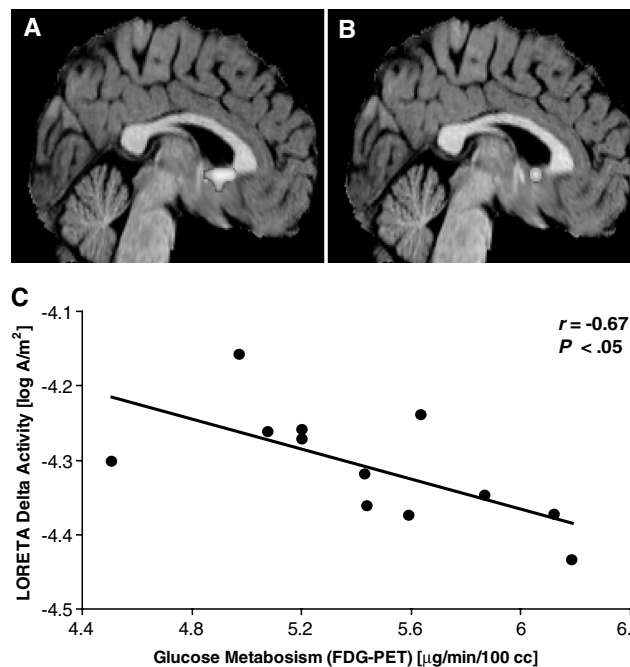

Figure 3.2. Reciprocal relation between delta activity and glucose metabolism. In a recent study integrating concurrently recorded electric (28-channel scalp EEG) and metabolic ([^{18}F]-2-fluoro-2-deoxy-D-glucose positron emission tomography, FDG-PET) measures of brain activity, melancholic depression was characterized by (A) significantly increased delta current density (see yellow-red colors), as assessed with LORETA (see Section 8.2.3.); and (B) significantly decreased glucose metabolism (see blue colors). Statistical maps are thresholded at P < .05 (corrected) and displayed on a representative structural MRI. In psychiatrically healthy subjects, a significant negative correlation between delta current density and glucose metabolism in the subgenual prefrontal cortex emerged (C). Adapted from Pizzagalli et al. (2004) with permission.

3.1. Delta band (1–4 Hz)

Delta oscillations reflect low-frequency activity (1–4 Hz) typically associated with sleep in healthy humans and neurological pathology. In adults, delta power has been shown to increase in proximity of brain lesions (Gilmore & Brenner, 1981) and tumors (Fernandez-Bouzas et al., 1999), during anesthesia (Reddy, Moorthy, Mattice, Dierdorf, & Deitch, Jr., 1992), and during sleep (Niedermeyer, 1993). Moreover, inverse relationships between delta activity and glucose metabolism have been reported in both pathological (e.g., dementia; Szelies, Mielke, Kessler, & Heiss, 1999) and normal (Pizzagalli et al., 2004) conditions. In our own study, an inverse relationship between delta current density (assessed via an EEG distributed source localization technique) and glucose metabolism (assessed via PET) was found within the subgenual prefrontal cortex (Figure 3.2). Delta is also the predominant activity in infants during the first two years of life. Ontologically, slow delta and theta activity diminish with increasing age, whereas the faster alpha and beta bands increase almost linearly across the life span (e.g., John et al., 1980).

Collectively, these findings suggest that delta activity is mainly an inhibitory rhythm.

3.2. Theta band (4–8 Hz)

Theta activity refers to EEG activity within the 4–8 Hz range, prominently seen during sleep. During wakefulness, two different types of theta activity have been described in adults (Schacter, 1977). The first shows a widespread scalp distribution and has been linked to decreased alertness (drowsiness) and impaired information processing. The second, the so-called frontal midline theta activity, is characterized by a frontal midline distribution and has been associated with focused attention, mental effort, and effective stimulus processing. Recent studies have implicated the anterior cingulate cortex (ACC) as a potential generator of frontal midline theta activity (e.g., Asada, Fukuda, Tsunoda, Yamaguchi, & Tonoike, 1999; Luu, Tucker, Derryberry, Reed, & Poulsen, 2003; Onton, Delorme, & Makeig, 2005). Consistent with these findings, in a recent study integrating electrical (EEG) and metabolic (PET) measurements of brain activity, we found that the ACC (Brodmann area 24/32) was the largest region with significant positive correlations between theta current density and glucose metabolism (Pizzagalli, Oakes, & Davidson, 2003).

Physiologically, the septo-hippocampal system has been strongly implicated in the generation of theta oscillations, although theta has also been recorded in numerous other limbic regions, including the ACC, entorhinal cortex, and the medial septum, among others (Vinogradova, 1995; Bland & Oddie, 1998). In rodents, generation of hippocampal theta activity is crucially dependent on afferents from the medial septum/vertical limb of the diagonal band of Broca complex (MS/vDBB), which is considered the pacemaker of hippocampal theta (Vertes & Kocsis, 1997). Additional evidence suggests that theta can be generated in the cingulate cortex independently of the hippocampal system (e.g., Borst, Leung, & MacFabe, 1987). In light of the observation that these oscillation facilitates transmission between different limbic structures, it has been speculated that theta activity may subserve a gating function on the information processing flow in limbic regions (Vinogradova, 1995).

3.3. Alpha band (8–13 Hz)

The alpha rhythm refers to EEG activity within the 8–13 Hz range. In healthy adults, alpha activity typically has amplitude between 10 and 45 μV, and can be easily recorded during states of relaxed wakefulness, although large individual differences in amplitudes are not uncommon (Niedermeyer, 1993). Topographically, alpha rhythms show their greatest amplitude over posterior regions, particularly posterior occipito-temporal and parietal regions, and can best seen during resting periods in which the subjects has his/her eyes closed. In fact, alpha rhythm can be greatly diminished or abolished by eye opening, sudden alerting, and mental concentration, a phenomenon known as alpha blockage or alpha desynchronization. The alpha rhythm can also be attenuated when alertness decreases to the level of drowsiness; this attenuation is, however, often accompanied by a decrease in frequency.

The physiological role of alpha rhythm remains largely unknown. Traditionally, the posterior distribution of these oscillations and the observation of alpha blockade with eye opening have been interpreted as suggesting that alpha may be associated with visual system functions emerging in the absence of visual input (Fisch, 1999). Indeed, some authors have expanded upon this notion by suggesting that alpha synchronization may represent an electrophysiological correlate of cortical "idling" or cognitive inactivity (e.g., Pfurtscheller, Stancak, Jr., & Neuper, 1996). In recent years, this conjecture has been heavily debated in the literature, particularly in studies investigating evoked EEG activity, in which alpha synchronization has been described during information processing (e.g., Cooper, Croft, Dominey, Burgess, & Gruzelier, 2003; Klimesch, 1999). Further complicating the physiological interpretation of alpha, emerging evidence indicates that different alpha sub-bands may be functionally dissociated, in particular with increasing task demands (Fink, Grabner, Neuper, & Neubauer, 2005). Specifically, in cognitive tasks, lower alpha (e.g., 8–10 Hz) desynchronization (suppression) has been associated with stimulus-unspecific and task-unspecific increases in attentional demands (e.g., Klimesch, 1999). Upper alpha (e.g., 10–12 Hz) desynchronization, on the other hand, appears to be task-specific, and it has been linked to processing of sensory-semantic information, increased semantic memory performance, and stimulus-specific expectancy (Klimesch, 1999).

3.4. Beta band (13–30 Hz)

Traditionally, lower-voltage oscillations within the 13–30 Hz frequency range have been referred to as beta. In adults, beta activity has amplitudes between 10–20 μV, presents mainly a symmetrical fronto-central distribution, and typically replaces alpha rhythm during cognitive activity. Consistent with this view, beta rhythm has been shown to increase with attention (Murthy & Fetz, 1992) and vigilance (Bouyer, Montaron, Vahnee, Albert, & Rougeul, 1987), for example. Collectively, these findings suggest that beta increases generally reflect increased excitatory activity, particularly during diffuse arousal and focused attention (Steriade, 1993).

3.5. Gamma band (36–44 Hz)

Gamma oscillations have been associated with attention, arousal, object recognition, top-down modulation of sensory processes, and, in some cases, perceptual binding (i.e., the brain's ability to integrate various aspects of a stimulus into a coherent whole; Engel, Fries, & Singer, 2001).

Various findings indicate that gamma activity is directly associated with brain activation. First, human intracortical EEG studies have reported increased gamma oscillations during various mental processes, including perception (Rodriguez, Lachaux, Martinerie, Renault, & Varela, 1999) and learning (Miltner, Braun, Arnold, Witte, & Taub, 1999). Second, dose-dependent decreases of gamma activity have been described during anesthesia (Uchida et al., 2000). Third, systematic decreases in gamma activity have been described throughout the sleep-wake cycle (highest during wakefulness, intermediate during REM sleep, and lowest during slow wave sleep; Gross & Gotman, 1999). A recent study from our laboratory using concurrent EEG and PET measurements provided further support for the notion that gamma is a direct indicator of activation because this band had the highest number of positive correlations between current density and glucose metabolism (Oakes et al., 2004).

Although the functional role of gamma oscillations needs to be more fully elucidated, these oscillations are assumed to reflect large-scale integration of and synchrony among widely distributed neurons, particularly in states of diffusely increased vigilance (e.g., Mann & Paulsen, 2005; Steriade, 1993). Physiologically, various mechanisms have been implicated in the generation of gamma oscillations, including: (1) intracortical circuitries, in particular those involving distant brain regions; (2) synaptic interactions among the cortex, thalamus, and limbic structures; and (3) brainstem-thalamic cholinergic activation (Steriade, 1993). Notably, recent animal and human findings have shown that gamma and theta oscillations can be functionally coupled both during activated (task-related) and resting (task-free) states (e.g., Fell et al., 2003; Mann et al., 2005; Schack, Vath, Petsche, Geissler, & Moller, 2002). In general, these studies have shown that gamma bursts occur within periods of the theta phase (Buzsaki, 1996 for review). Consistent with this notion, in a recent 128-channel source localization EEG study (Pizzagalli, Peccoralo, Davidson, & Cohen, 2006), we found significant positive correlations between resting theta and gamma current densities within various subdivisions of the ACC (correlation range: 0.51–0.59).

4. DATA ACQUISITION AND SIGNAL ANALYSIS

In the following sections, a selected discussion will be presented of issues associated with data acquisition and signal processing (for more in-depth reviews, see Davidson et al., 2000; Pivik et al., 1993; Gasser & Molinari, 1996; Nuwer et al., 1999; Thakor et al., 2004).

4.1. Electrodes

4.1.1. Electrode locations and high-density recordings
EEG signals always represent the potential difference between two electrodes, an active electrode and the so-called reference electrode. Accordingly, it is clear that the
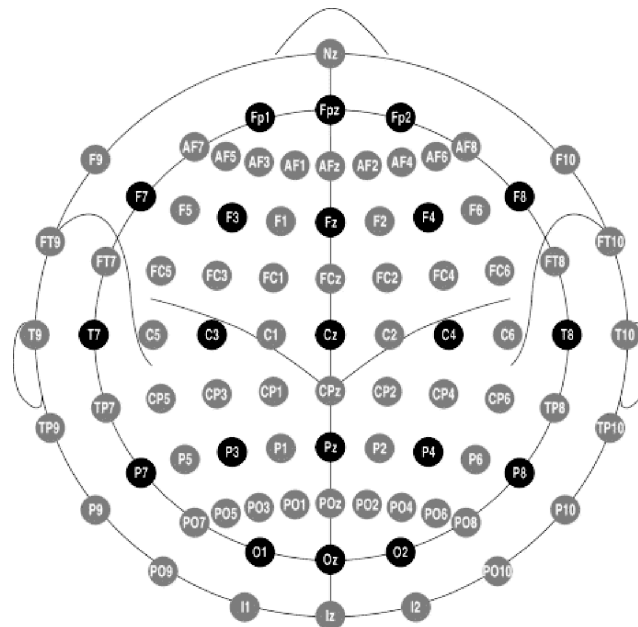

Figure 3.3. Electrode positions and labels in the International 10–20 System. Black circles denote electrode positions and labels from the 10–20 system; gray circles denote additional electrode positions and labels introduced with the 10–10 system. Reprinted from Clinical Neurophysiology, Vol. 112, Oostenveld, R. & Praamstra, P., The five percent electrode system for high-resolution EEG and ERP measurements, pp. 713–719, Copyright (2001), with permission from International Federation of Clinical Neurophysiology.

quality of EEG signals is dependent on the integrity of the electrode-electrolyte-skin interface (for a summary of clinical and experimental electrodes, see Fisch, 1999). Irrespective of their material, EEG electrodes should not attenuate signals between 0.5 and 70 Hz. To allow comparisons among studies it is important to adhere to standardized electrode locations. For many years, the accepted system for electrode placement has been the International 10–20 system proposed by Jasper (1958). The name refers to the fact that electrodes are placed at sites 10% and 20% from four fiduciary points (nasion, inion, left, and right mastoids); this placement schema allows positioning of 19 electrodes homogenously across the scalp. In recent years, this system has been extended to the so-called 10–10 system (American Electroencephalographic Society, 1991) and the 5–5 system (Oostenveld & Praamstra, 2001), in which intermediate positions between those of the 10–20 system have been derived (Figure 3.3).

In recent years, high-resolution EEG systems with numbers of electrodes ranging from 64 up to as many as 256 have been introduced, with the goal of increasing the spatial sampling of the EEG (e.g., Gevins et al., 1994; Tucker, 1993). In one particular dense-array system (Tucker, 1993), scalp abrasion prior to the application of EEG electrodes is not necessary, reducing (a) the electrode application time (e.g., 15-min time for applying a 128-channel EEG net); (b) subject's discomfort; and (c) risk of infections. Instead, these systems are simply soaked in a saline

(electrolyte) solution and then applied directly to the head (but see Greischar et al., 2004 for potential issues associated with electrolyte spreading in high-density recordings). The use of high-input impedance (200 MΩ) amplifiers allows the recording of reliable EEG traces with impedances one order of magnitude higher than the traditional 5 KΩ.

Studies using simulated as well as real EEG data have suggested that an electrode distance of 2–3 cm is required to prevent distortions of the scalp potential distribution, and thus allow resolution of spatially focal EEG patterns (e.g., Srinivasan et al., 1998). In addition, recent studies assessing the role of spatial density (i.e., number of electrodes) on *source reconstructions* have clearly shown an improved spatial resolution with high-density recordings. In a simulation study, Lantz, Grave, Spinelli, Seeck, & Michel (2003) reported that the source localization accuracy increased linearly from 25 to 100 electrodes but reached a plateau after 100 electrodes. In the same study, Lantz and coworkers also showed a marked improvement in localization precision of the epileptic sources when increasing electrodes from 31 to 63; again, at least in the case of spatially focal sources in epileptic patients, the improvements in localization accuracy were less dramatic when going from 63 to 123. Similar findings were reported by Luu et al. (2001), who investigated the role of electrode density in the ability to localize scalp abnormalities associated with acute cerebral ischemia. Using sensor downsampling (128, 64, 32, and 19 electrodes), the authors found that only 64 and 128 electrode arrays were capable of resolving spatially localized EEG abnormalities. As in Lantz et al., minimal gain was achieved when moving from 64 to 128 electrodes. Note however that, because Lantz et al. used a source localization technique (EPIFOCUS; Grave de Peralta, Gonzalez, Lantz, Michel, & Landis, 2001) that assumes a single focal source, distributed source localization techniques (see Section 8.2) may benefit from the additional spatial sampling achieved with >100 electrodes. Consistent with this hypothesis, Michel et al. (2004) found that source imaging with 128-channel EEG epileptic spike data led to correct localization (to the order of the affected lobe) in 93.7% of the focal epileptogenic area, as independently assessed through presurgical assessments.

Regardless of the number of electrodes utilized, uniform and homogenous coverage of the scalp is of paramount importance for reliable measurements of the scalp potential field, a critical prerequisite for any source localization technique (Michel et al., 2004). Moreover, measurements of exact 3-D electrode position with a digitizer (if available) may provide important information to account for individual differences in electrode positioning (e.g., Towle et al., 1993). Recently, a solution based on photogrammatic measurements has been developed for quick and accurate measurement of electrode positions in high-density EEG system (Russell, Jeffrey, Poolman, Luu, & Tucker, 2005). In this approach, multiple cameras are used to record the location of individual sensors, allowing for the reconstruc-

tion of the 3-D sensor positions. In sum, both simulation and experimental studies suggest that at least 60 (preferably more) equally distributed electrodes are required for accurate spatial sampling of scalp activities.

4.1.2. Electrode interpolation

The importance of spatial sampling for source localization is associated with the issue of how best to deal with electrodes with corrupted EEG signals due to excessive artifacts or technical malfunction. As mentioned above, source localization strongly relies on the scalp potential distribution, which itself can be distorted by uneven spatial sampling. Consequently, simply omitting corrupted electrodes is not a feasible solution, and interpolation methods are needed. Broadly speaking, two interpolation methods have been utilized: linear (nearest neighbor) and spline interpolation methods (e.g., Perrin, Pernier, Bertrand, & Echallier, 1989). In the first method, corrupted activity is reconstructed through a weighted average using data from neighboring electrodes (the weights are proportional to the Euclidian distance between the electrodes). With the spline interpolation method, information from all sensors is used to represent the overall potential distribution on the entire scalp, and thus to reconstruct the activity at missing channels. Although mathematically simpler, linear interpolations have the disadvantage that (a) edge electrodes cannot be accurately estimated; (b) only a few electrodes are used; and (c) maxima and minima of activity are always located at electrode sites (Maurer & Dierks, 1991). Empirical evidence indicates that non-linear spline interpolation methods achieve greater accuracy (Soufflet et al., 1991).

4.1.3. Recording reference choice

As mentioned in Section 4.1.1, EEG waveforms represent the *differential* voltage between a given electrode and the recording reference. It is therefore clear that the choice of reference completely determines EEG waveforms (Lehmann, 1987; Dien, 1998), an important methodological consideration that all too often is still not recognized in the EEG literature. For example, recording with a vertex (Cz) reference would lead to small EEG deflections in the proximity of Cz due to potential synchronization of firing activities within closely spaced brain regions and volume propagation of the EEG signal. Similarly, recording with mastoid or linked ears montage would lead to rather small waveforms at electrodes positioned over temporal brain regions (Pivik et al., 1993).[3]

Ideally, the reference electrode should be electrically inactive, allowing the measurement of an absolute EEG value. Both cephalic and noncephalic references are never electrically inactive, and thus contribute to recorded EEG signals. Understanding this point is particularly important when deciding the location to the recording reference in

---

[3] Note, however, that information contained in the reference (e.g., Cz) is not permanently lost, but can be recovered by recomputing the EEG data against a different reference electrode.

order to avoid situations in which the reference itself is contaminated by noncephalic activity (e.g., muscle or electrocardiogram artifacts). In these circumstances, because the potential difference is measured between the active and reference electrodes, substantial artifacts would be introduced in all EEG channels.

Due to the fundamental issue of reference-dependency of EEG waveforms, reference-free transformations have been proposed for an unbiased assessment of EEG measures. In particular, the use of an average reference (Lehmann, 1987), radial current flow (Hjorth, 1975), and current source density (Perrin, Bertrand, & Pernier, 1987) have attracted substantial interest. With the average reference approach, at each moment in time, EEG signals are re-derived against the average value across all electrodes. In the Hjorth's method, also known as source derivation or Laplacian transformation, the average potential difference between each electrode and the nearest four electrodes is computed.[4] By computing the density of local radial currents, this approach acts as a spatial high pass filter and emphasizes shallow cortical generators. Finally, current source density (also known as surface Laplacian) is computed as the second derivative of the voltage surface; by acting also as a spatial filter, surface Laplacians can be helpful in identifying focal patterns (Nunez & Pilgreen, 1991). Although these reference-free methods have been successfully used in the literature for an unbiased assessment of EEG signals, it is important to stress that they often require a relatively high number of electrodes (e.g., 32 electrodes or above), as well as homogenous electrode distribution across the scalp for reliable estimates (Pivik et al., 1993).

Although the choice of the reference electrode greatly influences *waveform* analyses, it is important to note that the reference choice is completely irrelevant for *any* source localization. In fact, the spatial configuration of the scalp potential distribution is independent of the reference electrode (the reference merely affects the zero line; Lehmann, 1987). As source localization relies on the spatial distribution of the scalp EEG and ERP, different reference montages (e.g., average reference, linked mastoids) lead to identical estimates of intracerebral sources.

4.2. Recording: Filters and sampling rate

The bandwidth of the EEG signal is 0.1–100 Hz in frequency, although most studies focus on frequencies below 30 Hz (or below 50 Hz if gamma activity is investigated). Although a comprehensive review of calibration, filtering, and digitization of EEG signals is beyond the scope of this chapter (see Davidson et al., 2000; Pivik

et al., 1993; Dumermuth & Molinari, 1987 for excellent reviews), some points should be emphasized here. First, the extent to which the digital signal under investigation accurately reflects the physiological (analog) signal completely depends on the sampling rate. As a general rule, the sampling rate should be at least twice the highest frequency present in the signal under investigation. This rule, also known as the *Nyquist Theorem*, prevents the introduction of spurious low-frequency components into the signal, a phenomenon called *aliasing* (Dumermuth & Molinari, 1987). Aliasing occurs when a signal is sampled at a rate that is too low, and introduces irreparable distortion to the digital waveform (Figure 3.4). Two methods can be used to avoid aliasing. First, frequencies higher than half the sampling rate should be removed from the EEG before digitization occurs (e.g., by using an analog or hardware filter). Second, high sampling rates (e.g., four-fold greater than the filter cutoff frequency) could be used. Because the EEG signals of interest is typically between 1 and <60 Hz, a sampling rate of 250 Hz with an analog 0.1–100 Hz filter are appropriate for most EEG studies. If contamination of low frequency artifacts is an issue, the high pass analog filter can be set as high as 1 Hz (Nuwer et al., 1999). Higher sampling rate is required to investigate early sensory ERP components or high-frequency EEG patterns.

4.3. Artifacts

When recorded, the raw EEG signal is virtually always contaminated by various sources of noise and artifacts. In general, biological and non-biological artifacts can be differentiated (see pp. 107–121 in Fisch, 1999 for illustrations of most common artifacts). The former mainly derive from subject's movements, muscle activities, blinks, eye movements, heartbeat, and sweating. As will be discussed later, concurrent recording of the electrocardiogram (ECG), electrooculogram (EOG), and electromyogram (EMG) can be very important for a proper detection and removal of these artifacts. Nonbiological artifacts primarily derive from interferences from power lines (50/60 Hz), additional electrical noise, poor subject grounding, and poor electrode contact. One common source of 50/60 Hz noise stems from fluorescent lights. Use of notch filters (50/60 Hz), proper subject grounding, and shielding of the recording system can greatly diminish the influence of nonbiological artifacts. Proper grounding, in particular, can substantially improve the quality of the EEG signals and avoid leakage of current from the EEG system to the subjects.[5] Often, a midforehead electrode is used for this purpose.

Visual and, increasingly more often automatic, offline artifact detection is essential before any EEG analyses, and substantial expertise is required for a proper differentiation of normal and contaminated EEG activity. Drowsiness can introduce a substantial confound in baseline EEG

---

[4] For instance, assume that a researcher wishes to compute the Laplacian transformation at electrode Cz, which has a potential value of 10 μV, and that the four neighboring electrodes Fz, C3, Pz, and C4 have potentials of 3, 5, 12 and 5 μV, respectively. The new source-derivation value for Cz would be 3.75, i.e., [(Cz-Fz) + (Cz-F3) + (Cz-Pz) + (Cz-C4)]/4.

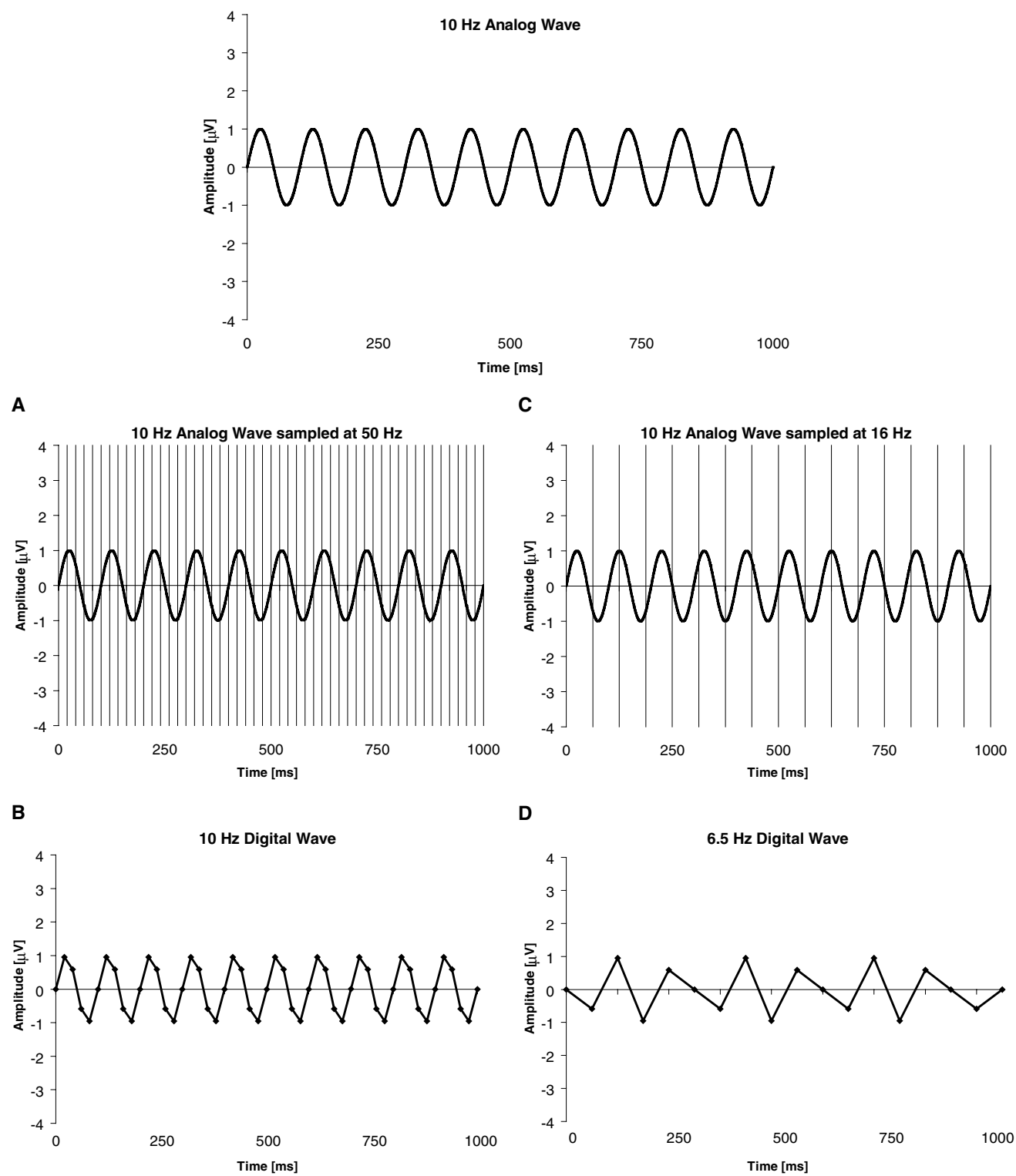[5] Grounding can be achieved by connecting participants to the ground of the amplifier system.

Figure 3.4. Example of aliasing due to insufficient sampling rate. A 10 Hz sine waveform is digitized at two different sampling rates. (A) The sampling rate (50 Hz) is greater than twice the waveform frequency, which results in (B) an appropriate digital representation of the analog signal. (C) The sampling rate (16 Hz) is less than twice the waveform frequency, yielding (D) a false (aliased) representation of the analog signal. Note how undersampling introduces an irreparable lower frequency component in the digital signal. Modified after Fisch (1999).

recording due to a global change in the functional brain state. Typically, EEG slowing over anterior regions, slowing and subsequent decrease of alpha activity, and slow eye movement (particularly horizontal), are associated with subject's drowsiness. When this pattern is detected, it is recommended to exclude these periods of EEG (Pivik et al., 1993).

Removal of ECG and EOG artifacts is particularly important, because these artifacts overlap in frequency and amplitude with the EEG. In humans, normal ECG is within the 1–1.5 Hz range, suggesting that its second-order harmonics (2–3 Hz) is within the delta range (Thakor et al., 2004). Blinks and eye movements mostly generate activity within the delta and theta range (i.e., <7.5 Hz). Blinks, which typically last 200–400 ms and can generate artifacts with an amplitude up to 800 μV, can however also affect the alpha band (and to a lesser extent the beta band), in particular at anterior sites (Hagemann & Naumann, 2001). For proper detection of ocular artifacts, it is essential to utilize additional channels to record vertical and horizontal eye movements. To record vertical eye movement, two electrodes are affixed below and above one eye; for horizontal movements, two electrodes are affixed at the extremities of an eye. Over the years, several methods have been described in the literature to detect *and* correct both sources of noise (see Croft, Chandler, Barry, Cooper, & Clarke, 2005 for a recent review and comparison of the most widely used EOG correction algorithms).

Artifacts originating from muscle activity can contaminate a broad range of EEG frequencies because the primary energy in EMG signals is between 10 and 200 Hz (Tassinary & Cacioppo, 2000). Due to this overlap with EEG frequencies, occurrence of these artifacts are particular problematic for EEG analyses. Contamination from muscle activity can be troublesome for studies interested in gamma activity, which can be easily influenced by noncephalic, myogenic sources. Considering the explosion in interest in the functional role of gamma activity in mental processes, it is clear that proper attention must be devoted to the issue of EMG contamination to the gamma band. Due to frequency overlap, removing muscle artifacts through filtering can greatly distort real EEG signals. Accordingly, several authors proposed the use of regression approaches for dealing with this issue (e.g., Allen, Coan, & Nazarian, 2004; Davidson et al., 2000). In this approach, activity in higher frequencies (e.g., 50–70 Hz) is typically taken as a marker of muscle artifact, and its variance is removed using regression analyses or entered as covariate in analyses of variance (ANOVA).

In recent years, the method of independent component analysis (ICA) has been increasingly used for removal of ECG and other artifacts (see Makeig, Bell, Jung, & Sejnowski, 1996 for a tutorial). In view of the fact that artifacts typically do not occur time-locked to a given event or evoked response, ICA is ideally suited to remove such interfering signals. Consistent with this notion, ICA works best when applied to unaveraged (raw) EEG data. In the

case of ECG, contaminated EEG is entered into the ICA, which separates the EEG and EOG components. In a subsequent step, the ECG component is set to zero in the coefficient matrix leading to a removal of ECG artifacts. ICA approaches have been also used to remove EOG artifacts (Thakor et al., 2004).

5. QUANTITATIVE SCALP ANALYSES

The introduction of computers has enabled the development of several methods to investigate EEG signals with respect to various parameters, including waveform frequencies, amplitudes, phase, and coherence. Quantitative EEG (qEEG) analyses can be divided into linear and nonlinear approaches. Among the most widely used linear methods to quantify spontaneous or task-related EEG activity are spectral and coherence analyses, which typically assume that the EEG signals are stationary processes.[6] Nonlinear approaches, which often incorporate higher order statistics, information theory, or chaos theory, started to emerge in the 1990s, and have demonstrated their usefulness particularly when applied to transient and irregular EEG patterns (see Thakor et al., 2004 for a review).

5.1. Spectral analyses

Spectral analyses are based on the notion that any oscillatory activity can be characterized by the sum of different sinusoidal waves with distinct frequencies and amplitude (see Figure 3.5 for a simulation). The goal of spectral analyses, which are often performed using the Fast Fourier Transform (FFT), is to estimate the contribution of various frequencies on the measured EEG signal. Commonly, spectral estimates are computed for discrete frequencies (e.g., 8.5–10 Hz for lower alpha). For a given frequency or discrete EEG band, the root-mean-square average amplitude or the power (the square of the amplitude) is used to quantify its contribution to the measured EEG signal. Mathematically, the Fourier coefficients indicate the strength of the signal at a given frequency.

In a typical EEG study, all available artifact-free EEG segments are entered in spectral analyses. When selecting the length of the artifact-free EEG segments, it is important to understand that this variable determines the maximal frequency resolution available for the analyses. Thus, selection of 2-sec segments will provide a 0.5 Hz resolution (i.e., the inverse of 2 sec), allowing to resolve, for example, 10 and 10.5 Hz frequencies. Note, however, that spectral analyses assume that the EEG is a stationary signal. Accordingly, segments entered in FFT analyses cannot be too long because of potential violation of the stationarity assumption (Gasser & Molinari, 1996). When relatively short segments are considered (e.g., <3.5 sec), the

---

[6] In simple terms, stationarity implies that the statistical proprieties of an EEG signal (e.g., mean, variance) do not vary over time.

A

1.5 Hz wave

B

7 Hz wave

C

20 Hz wave
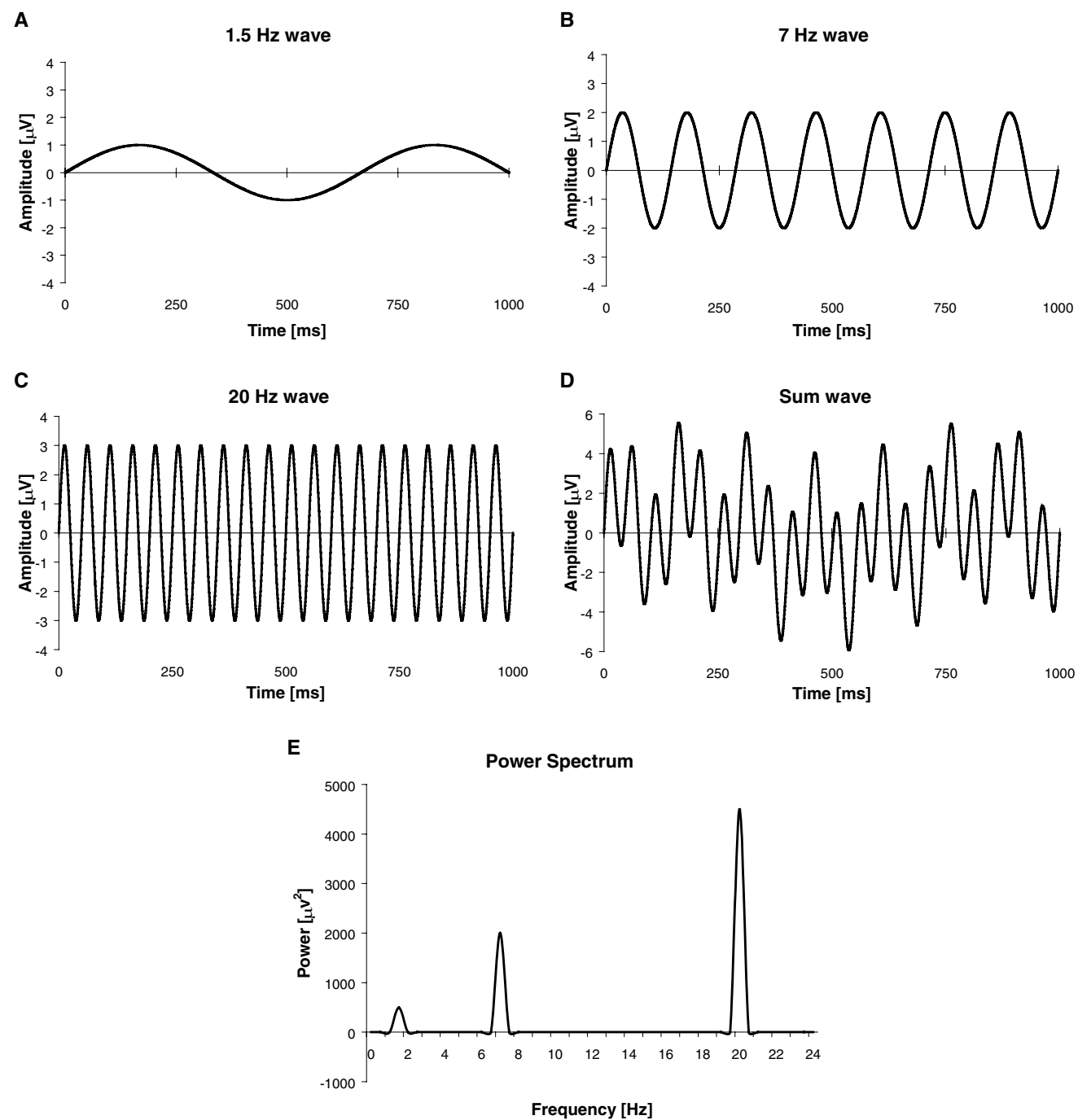
D

Sum wave

E

Power Spectrum

Figure 3.5. Simulation of power spectrum computation through Fast Fourier Transformation (FFT). In (A), (B), and (C), simple sine waves oscillating at 1.5, 7, and 20 Hz are shown. In (D), the sum of these three sine waves is shown. In (E), the results of an FFT analysis of the complex waveform displayed in (D) are shown. Not surprisingly, the spectrum identifies frequency peaks at 1.5, 7, and 20 Hz.

stationarity assumption is typically met in spontaneous EEG recording.

To allow reliable estimation of spectral features and to reduce the impact of second-to-second variability in EEG signals, at least 60 sec of artifact-free data should be used for spectral analyses (Nuwer et al., 1999; Pivik et al., 1993). Further, to avoid introduction ("leakage") of spurious fre-

quencies arising from abrupt changes in EEG signals at the beginning and the end of the EEG segments, a so-called taper transformation should be used. For this purpose, the Hanning (cosine) window has been commonly utilized. This window tapers the beginning and end of the EEG segment to zero, whereas the middle of the segment retains 100% of its amplitude (see Dumermuth & Molinari, 1987

for a review of various windowing approaches). Because the use of windowing reduces the amount of data that can be analyzed within a segment, overlapping segments (e.g., 50%) are often used to restore the amount of data for spectral analyses.

Although we refer to prior reviews for a comprehensive discussion of spectral analyses (e.g., Gasser & Molinari, 1996; Davidson et al., 2000, several important methodological points should be emphasized here. First, an under-appreciated issue is that the frequency range for a given oscillatory activity (e.g., alpha activity) can show substantial individual differences. Klimesch (1999) has long advocated the use of individually defined frequency ranges and has shown in several experimental situations that this choice can have substantial effects on the findings. Second, measures of *absolute* or *relative* power can be derived from spectral analyses. Whereas absolute power reflects the amount of a given frequency within the EEG, relative power is calculated as the amount of EEG activity in a given frequency band divided by the total power. In general, absolute power should be preferred because it can be more easily interpreted. Third, when dealing with power data, transformations (e.g., log) are often used before statistical analyses to approximate a Gaussian distribution (Davidson et al., 2000). Finally, ratios or difference scores are often computed between different electrodes in an attempt to draw inferences about differential hemispheric activation. Conceptual and methodological considerations concerning these asymmetry metrics are discussed next (for reviews, see Allen et al., 2004; Coan and Allen, 2004; and Davidson et al., 2000).

5.1.1. Asymmetry metrics

In many experimental situations, psychophysiologists are interested in investigating whether the two brain hemispheres are differentially involved in specific cognitive and affective processes, personality traits, or various forms of psychopathology. Although many metrics have been used to investigate hemispheric differences (Pivik et al., 1993), the alpha power asymmetry index has been among the most commonly used. This index is derived from subtracting the natural logarithm of the left hemisphere power value from the natural logarithm of the right hemisphere power value (ln R – ln L). Because alpha power is considered to be inversely related to brain activation, positive numbers on this index indicate relatively greater left activity, whereas negative numbers denote relatively higher right activity.

The investigation of frontal EEG asymmetry has received particular attention, and over 80 studies have examined its role in emotion, motivation, and psychopathology (for a recent review, see Coan & Allen, 2004). In general, the picture emerging from this literature is that frontal EEG asymmetry is associated with (a) state-dependent emotional reactivity; (b) individual differences in emotional reactivity; and (c) individual differ-

ences in risk for a variety of emotion-related disorders (e.g., depression, anxiety). Conceptually, it has been proposed that left prefrontal regions might be implicated in a system that facilitates appetitive behavior and certain forms of affect that are approach-related. Conversely, right prefrontal regions have been implicated in withdrawal-related, negative affect (Davidson, 2004).

From a methodological perspective, the use of asymmetry metrics has several advantages. First, they allow researchers to control for individual differences in skull thickness, a variable that can artificially cause individual differences in scalp power values. Second, asymmetry metrics can increase statistical power by reducing individual differences in overall activity, and limit the number of statistical tests performed. Third, the internal reliability of the alpha power frontal asymmetry index is high, ranging from 0.76 to 0.93 across studies, and the test-retest reliability is acceptable (e.g., 0.69–0.84 across three weeks) (Allen et al., 2004). When asymmetry scores are reported, however, follow-up analyses assessing the unique contribution of each hemisphere to the asymmetry index should be presented. For example, a finding of relatively increased right frontal activity in a given patient population, although an important first step, should be subjected to further analyses to ascertain whether this pattern is due to (1) an increase of right frontal activity; (2) a decrease of left frontal activity; or (3) a combination of the above. From a statistical perspective, a laterality effect can only be claimed if the *Group × Hemisphere* or *Condition × Hemisphere* interaction is significant (Allen et al., 2004; Davidson et al., 2000).

5.2. Time-frequency analyses

From the last section it is clear that spectral analyses can provide important information about the frequency compositions of EEG oscillations. Spectral analyses cannot, however, provide any information about *when in time* such frequency shifts occur. Because the EEG is a dynamic, time-varying, and often non-stationary phenomenon, approaches allowing the investigation of transient changes in the frequency domain appear particularly important. To achieve this goal, various time-frequency analyses methods have been developed, including (a) short-time Fourier Transform (STFT), which allows to compute an FFT-based time-dependent spectrum (so-called spectrogram); and (b) wavelet analyses, which allow a more adaptive time-frequency approach affording flexible resolution. Wavelet analyses, in particular, have gained popularity in recent years due to their ability to accurately resolve EEG waveforms into specific time and frequency components (see Samar, Bopardikar, Rao, & Swartz, 1999 for a nontechnical tutorial). In this approach, EEG signals are viewed as shifted and scaled versions of a particular mathematical function (the wavelet), rather than a composition of sine waves with varying frequencies as in the FFT.

5.3. Coherence analyses

As summarized in Section 2.3., neurophysiological studies have demonstrated the presence of both local-scale synchronizations (i.e., synchronization among neighboring neurons) as well as large-scale synchronizations (i.e., synchronization among distant regions; e.g., Bressler & Kelso, 2001; Llinas, 1988). In EEG studies, the investigation of large-scale neuronal synchronization appears particularly important in experimental situations hypothesized to recruit distributed neuronal network. In order to quantitatively measure the dynamic functional interactions among EEG signals recorded at different scalp locations, *coherence measures* can be computed (Nunez et al., 1997).

Coherence is a frequency-dependent measure, mathematically obtained by dividing the cross-spectrum between two time series by the root of the two spectra (this computation is similar to a correlation; Schack et al., 2002). Cross-power spectrum is obtained by multiplying the Fourier transform of one signal with the complex conjugate of another signal, thus allowing the quantification of relationships between different EEG signals. Accordingly, coherence can range from 0, indexing the absence of any synchrony, to 1, indicating maximal synchrony between the frequency components of two signals, irrespective of their amplitudes.

Intriguingly, increased synchronization among distant regions has been observed within low-frequency oscillations (e.g., theta), whereas increased local synchronization has been observed for high-frequency oscillations (e.g., gamma; Buzsaki & Draguhn, 2004; von Stein & Sarnthein, 2000). In general, brain regions that are co-activated during a given cognitive process are assumed to show increased coherence ("neuronal synchronization") within specific EEG frequency bands, depending on the nature and difficulty of the task (Weiss & Mueller, 2003). For some authors, such coherence measurements have been interpreted as reflecting cortical interactions or connectivity (e.g., Thatcher, Krause, & Hrybyk, 1986). Consistent with this speculation, increased coherence has been generally observed with increased task complexity and efficient information processing, whereas pathological conditions characterized by dysfunctional networks (e.g., dementia, dyslexia) are characterized by decreased coherence (Leoncani & Comi, 1999; Weiss & Mueller, 2003).

Finally, it is important to note that, although coherence analyses assess the degree of synchronization between different brain regions, they cannot inform us about the *causality* of these interactions or the *direction* and *speed* of the information transferred. Only in recent years, advanced methods for assessing these important aspects of brain function have been described, including the Directed Transfer Function (DTF), the Directed Mutual Information (DMI), and the partial directed coherence (PDC) techniques (Thakor et al., 2004 for a review). In a recent study, Astolfi et al. (2005) presented a promising approach to estimate connectivity by applying structural equation modeling and DTF to cortical signals derived from high-resolution EEG recordings.

5.4. Quantitative EEG (qEEG)

In qEEG studies, also known as "neurometrics" (John et al., 1980), various variables derived from spectral and coherence analyses of multi-channel EEG recordings (e.g., absolute power, relative power, interhemispheric and intrahemispheric coherence, asymmetry scores) are entered into large normative, age-dependent databases in conjunction with demographic and clinical information. Age-regression qEEG equations and Z-scores are then utilized to (1) identify patterns of abnormal EEG patterns associated within specific neurological or psychiatric disorders; and (2) provide supportive evidence for differential diagnoses and treatment decisions (for a recent review, see Hughes & John, 1999). Recent studies have confirmed the ability of qEEG approaches of detecting abnormal EEG patterns in pathological conditions but also some of their limitations, which might in part derive, however, from the fact that clinical conditions are far from being homogenous entities. Thus, whereas abnormal qEEG patterns were found in 83% of 340 psychiatric patients but only in 12% of 67 controls, no EEG abnormality was specific to a given clinical entity, and patients with the same diagnosis often showed different EEG abnormalities (Coutin-Churchman et al., 2003).

5.5. EEG mapping and space-oriented EEG analyses

The advent of multi-channel EEG systems has fostered the development of EEG mapping techniques (Lehmann, 1987; Duffy, Burchfiel, & Lombroso, 1979 for seminal reviews). Conceptually, at a given moment in time, this method considers values at each electrode and through interpolation display the field distribution of brain electric activity. Unlike traditional EEG waveform approaches, EEG mapping considers data in the spatial domain first, and then in the temporal domain, providing a display of the constantly changing spatial distribution of bran activity (see Maurer & Dierks, 1991 for a tutorial). For topographic mapping, at minimum the complete 10–20 system should be used (i.e., >19 electrodes; Nuwer et al., 1999). One of the main advantages of space-oriented EEG analysis is that, at any given time point, activity from all electrodes is considered simultaneously. A second main advantage is that, unlike waveform analyses, space-oriented analysis is independent from the reference electrodes. In fact, the spatial configuration or landscape of a map does not change when a different reference is used. In a manner analogous to a geographical map, the topographical features, such as the location of maximum or minimum potential or the

potential gradients, are not affected by the chosen reference that defines the zero line.

Critically, when examining the unfolding of momentary potential distributions over time, one observes that these maps tend to remain relatively constant for some periods of time, and are then abruptly interrupted by the emergence of new landscapes (Lehmann, 1971). Lehmann (1990) called these temporal segments of quasi-stable map landscapes "microstates" and considered them the building blocks of human information processing. Note that different configurations of scalp potentials are assumed to index different functional brain states because (a) different scalp potential distribution must have been generated by different neural sources (Fender, 1987); and (b) different neural sources likely subserve different functions.

Consistent with this assumption that microstates index different functional brain states, studies have shown that different mental processes (Lehmann, Henggeler, Koukkou, & Michel, 1993) or arousal states (Cantero, Atienza, Salas, & Gomez, 1999) are associated with different microstate classes. Further converging evidence comes from the notable observations that different age groups can be characterized by distinctive patterns of changes in microstate durations and preponderance (Koenig et al., 2002). Such age-dependent microstate changes mirror comparable transitional stages classically described by developmental psychologists. Likewise, psychopathological conditions characterized by dysfunctional mental states, such as schizophrenia (e.g., Lehmann et al., 2005) or dementia (e.g., Strik et al., 1997), showed shortened durations for specific microstates. Intriguingly, in a recent study, Lehmann et al. (2005) reported that acute, medication-naïve, first-episode schizophrenic subjects had different "microstate syntax" (i.e., different microstate concatenations and transitions) as well as truncated duration for some microstates, raising the interesting possibility that this disease may be characterized by different concatenations of mental operations and precocious termination of information processing for certain types of mental operations. For methodological details about microstate analyses of EEG data, see Koenig et al. (2002) and Lehmann et al. (2005).

Although EEG mapping represents a powerful and unambiguous approach for scalp EEG data, it is important to stress that this technique does not provide any additional information about the generating sources underlying scalp measurements (Pivik et al., 1993). In Section 8, source localization techniques required for localization of intracerebral sources will be reviewed.

6. SURFACE-SOURCE IMAGING APPROACHES

6.1. Scalp Laplacian mapping

As mentioned in the Introduction, the spatial resolution of scalp EEG is limited by the blurring effects of the head

volume conductor. In fact, the head acts as a low-pass spatial filter, transmitting to the scalp broad, as opposed to focal, spatial patterns of activity (Srinivasan et al., 1998). Scalp Laplacian mapping can be used to restore high-frequency spatial information of brain electric activity that has been distorted by the low-conductivity skull (Hjorth, 1975; Nunez et al., 1997; Perrin et al., 1987). The surface Laplacian approach does not solve the inverse problem (i.e., it is not a 3-D source localization technique); rather it allows source mapping directly over the scalp surface. As reviewed by He (1999), surface Laplacian is thought to represent an approximation of the local current density flowing perpendicularly to the skull into the scalp (for this reason, it has been also called *current source density* or *scalp current density*). A further advantage of surface Laplacian methods is that they are reference-independent.

The scalp Laplacian was first introduced for EEG data by Hjorth (1975), who proposed a difference estimation scheme to calculate local Laplacian by using the potentials at surrounding electrodes (see Footnote 4). Although computationally easy to implement, this so-called local approach was found to have some limitations, including inaccurate estimation for large interelectrode distances and for border electrodes (He, 1999). To overcome these drawbacks, Perrin et al. (1987) introduced a global approach based on the mathematical modeling of the global scalp surface and a curvilinear coordinate system. In their implementation, Perrin and coworkers assumed that the scalp surface can be approximated by a sphere. Later, Babiloni et al. (1996) presented a solution called "realistic Laplacian estimator" that can be applied to any arbitrarily shaped scalp.

6.2. Cortical imaging

To increase the spatial resolution of the EEG, the cortical imaging approach can also be used to deconvolve the low-pass spatial filtering effects of head volume conduction (Gevins et al., 1994). In this approach, biophysical models of the passive conducting features of the head are used to deconvolve a scalp potential distribution into estimation of potentials or current dipole distribution at the superficial cortical surface (for review, He, 1999). Gevins and coworkers (1994), for example, presented a deblurring technique based on a realistic biophysical model of the passive conducting properties of the head to estimate the potential distribution at the cortical surface. To this end, a finite element model (see Section 7.1) based on MRI-reconstructed scalp, skull, and cortical surfaces was used. Conceptually, the rationale for this approach stems from the empirical observation that cortical pyramidal cells oriented perpendicularly to the cortical surface mainly contribute to the recorded scalp EEG signal (Speckmann et al., 1993). Note that neither the scalp Laplacian nor the cortical imaging approach are source localization techniques and thus are

unable to reconstruct sources in 3-D space. This important topic will be discussed next.

7. THE NEUROELECTROMAGNETIC FORWARD AND INVERSE PROBLEM

The "forward problem" refers to the process of estimating scalp potentials from intracranial current sources (Koles, 1998). If the configurations of intracranial sources and the conductivity proprieties of the tissues are known, then the scalp potential distribution can be calculated using basic physical principles. Therefore, the forward problem can be unambiguously solved. In contrast, the "inverse problem," the estimation of sources underlying scalp-recorded EEG data, is ill-posed. Although recording of the human EEG was first reported by Berger in 1929, it soon became evident that scalp-recorded electromagnetic measurements do not contain sufficient information about the 3-D distribution of the electric neuronal activity. As early as the mid-nineteenth century, Helmoltz (1853) had already described the nonuniqueness of this type of electromagnetic inverse problem: the current distribution inside a conducting volume cannot be uniquely determined by the field and potential information outside it. Thus, scalp-recorded EEG/MEG measurements can be explained by an infinite number of different generating distributions, even with an infinite numbers of recording electrodes (Fender, 1987). To understand this concept, consider that the inverse problem can be mathematically represented as:

$$D = GX + n \qquad (3.1)$$

where D is a vector representing the scalp-recorded potentials, X is an unknown vector representing the generating sources (the current density vector), n is noise, and G is the transfer matrix, which mathematically implements both the electromagnetic (e.g., conductivity values for the brain, skull, and scalp) and geometrical (e.g., shape) features of the solution space considered in the inverse solution ("the head volume conductor model"). The inverse problem refers to finding X given known D. Specifically, the main goal is to minimize the following function:

$$O(X) = ||D - GX||^2 \rightarrow \min \qquad (3.2)$$

In general terms, it is not possible to determine which solution among the infinite possibilities corresponds to the actual solution; consequently, the quest for developing an electromagnetic tomography appears, at first, hopeless. Fortunately, the EEG and MEG follow certain electrophysiological and neuroanatomical constraints, which when combined with the laws of electrodynamics, provide an approximate solution of the inverse problem (Baillet et al., 2001; Michel et al., 2004; Pascual-Marqui, Esslen, Kochi, & Lehmann, 2002). When considering Equation 1 it becomes immediately evident that the localization accuracy of *any* source localization technique is critically dependent on: (1) the head model used to compute the inverse solution;

and (2) the inverse solution itself (Michel et al., 2004). In the following section, these two important aspects will be reviewed, followed by a description of various solutions to the inverse problem currently used in the EEG literature.

7.1. Head volume conductor model

The head volume conductor model plays a critical role in source localization because it determines the way intracerebral sources give rise to the scalp-recorded signal. As indicated above, the head model mathematically implements both the electromagnetic and geometrical properties of the solution space. Over the years, three head models have been used: (1) three-spherical head model (e.g., Ary, Klein, & Fender, 1981); (2) a boundary element model (BEM; e.g., Hamalainen & Sarvas, 1989); and (3) a finite element model (FEM; e.g., Miller & Henriquez, 1990). In terms of complexity and computational burden, the spherical model represents the simplest, the BEM the intermediate, and the FEM the most complex model. BEM and FEM models are typically developed from high-resolution structural MRI scan of individual subjects and can better account for individual anatomical differences, providing therefore more realistic head models.

The three-spherical head model, which has been most frequently used, approximates the head as a set of nested concentric and homogenous spheres, in which the skull, scalp, and brain are modeled as different layers with different conductivity. Typically, standard conductivity values, which have been measured in separate studies from excised tissue, are used for the different compartments, but in recent years attempts to assess conductivities through diffusion tensor MR imaging have begun to emerge (e.g., Tuch, Wedeen, Dale, George, & Belliveau, 1999). In general, spherical models can provide appropriate localization in superior regions of the brain, where the head shape approximates a sphere.

The BEM, in contrast, approximates different compartments of volume conductor models (e.g., skin, skull, cerebral spinal fluid) through closed triangle meshes with different conductivity values and dimension and thus attempts to take into account realistic geometry. Although the BEM clearly represents an improvement and more realistic model than the three-spherical head model, this model assumes homogeneity and isotropy within the head and brain. To cope with this potential issue, FEM models have been developed.

The FEM, unlike other methods, can account for the actual head shape and tissue discontinuities, and accommodate anisotropic tissue[7] in the conductivity model of the head volume, allowing detailed 3-D information on tissue conductivity for each region. This approach models current flow in an inhomogeneous volume by representing the conductor as a complex assemblage of many equally sized cubes or tetrahedrons. The use of tetrahedrons can

---

[7] Anisotropy refers to the property of having different values when measured in different directions.

accommodate elements that vary in size, thus allow modeling of the head geometry and anisotropy precisely. For several authors, the high computational efficiency of the BEM makes this model a valuable compromise between the oversimplifying sphere head volume model and the computationally intensive FEM model (He, 1999).

8. SOURCE LOCALIZATION TECHNIQUES

Estimating the sources of scalp-recorded electromagnetic activity has attracted considerable interest, and various solutions have been described in the literature. In general these solutions can be divided into two broad categories, *equivalent dipole approaches* and *linear distributed approaches*. The first approach typically assumes that EEG/MEG signals are generated by a relatively small number of discrete and focal sources, which can be modeled as single, fixed, or moving dipoles (e.g., Scherg & Ebersole, 1994). Through an iterative process, locations, orientations, and strength of these equivalent current dipole (ECD) are selected to minimize the difference between the predicted and the actual EEG measurements. The solution derived through this approach strongly relies on the numbers of dipoles; unfortunately, in many experimental situations, the numbers of dipoles cannot be determined a priori (e.g., Phillips, Rugg, & Friston, 2002a).

Distributed approaches, in contrast, consider all possible source locations simultaneously. In addition to the advantage conferred when no a priori assumptions about the numbers of sources are required, distributed approaches typically allow researchers to limit the solution space by means of anatomical and functional constraints. As will be discussed in the next section, anatomical constraints assume that some specific compartments (e.g., gray matter) or regions of the brain (e.g., cortical structures) have a higher likelihood of generating scalp-recorded EEG signals than others, and are thus essential for narrowing the search for a "unique" solution. In the following sections, a non-technical survey of various source localization techniques will be presented (for more technical reviews, see Baillet et al., 2001; Hamalainen & Ilmoniemi, 1994; Grave de Peralta & Gonzalez Andino, 2000; Phillips et al., 2002a; Phillips et al., 2002b; Pascual-Marqui et al., 2002; Trujillo-Barreto et al., 2004).

8.1. Equivalent dipole approaches (Dipole Source Modeling)

The equivalent current dipole (ECD) model is the most basic source localization technique and assumes that scalp EEG potentials are generated by one or few focal sources (for review, see Fuchs, Ford, Sands, & Lew, 2004). A dipole does not reflect the presence of a unique and discrete source but it is rather a mathematically convenient representation (i.e., the center of gravity) of synchronized activation of a large number of pyramidal cells likely extending larger patches of gray matter (Baillet et al., 2001). In fact,

a dipole is assumed to represent a patch of cortical gray matter layer containing approximately 100,000 pyramidal cells oriented in parallel to each other and activated simultaneously (Fuchs et al., 2004). Heuristically, the position of a dipole can provide clues about the extent and configuration of the activated cortical area (Lopes da Silva, 2004): superficial dipoles typically reflect localized cortical activity, whereas deeper dipoles reflect the activity of an extended cortical area.

In this approach, focal sources are modeled by an ECD through six parameters: three location parameters (X, Y, Z), two orientation parameters, and one strength (amplitude) parameter. Depending on the experimental procedures and/or a priori hypotheses, moving, fixed, or rotating dipoles can be used. Using an iterative procedure and nonlinear multidimensional minimization procedures, the inverse problem is solved by attempting to identify dipole parameters that best explain the observed scalp potential measurements (Fuchs et al., 2004). In its simplest terms, initial dipole parameters are selected, the forward solution is computed, and a least-square comparison between estimated and actual measurements is calculated. This process is continued until the difference between estimated and actual measurements is minimized. Without a priori assumption, one of the main concerns with this approach is that it can get trapped in local minima (Michel et al., 2004). Additionally, depending on the spatial configuration of the underlying sources, a dipole can sometimes be found at physiologically implausible locations, such as within white matter or even outside of the brain.

Over the years, various dipole source models have been developed, including the moving dipole model, rotating dipole model, regional dipole model, fixed (coherent) dipole model, and fixed (multiple signal classification or MUSIC) model (see Fuchs et al., 2004 for a review). Another interesting approach, called EPIFOCUS, has been recently proposed by Grave de Peralta et al. (2001). EPIFOCUS assumes a single focal source, but unlike single dipole modeling, does not assume that this source is spatially restricted to a single point. The *moving dipole model* assumes only one dipole at the time and allows all parameters to vary. The *rotating dipole model* constrains location to a single point but allows orientations and strength to vary. The *fixed dipole model*, in contrast, holds position and orientation constant within a given interval and it estimates the dipole strength for each time point. These subtle differences in these models, which are the ones most frequently used, underscore the need to incorporate prior neuroanatomical and neurophysiological knowledge to guide the selection of the physiologically most plausible model, making source reconstruction a hypothesis-driven process. In general, some caution should be exerted when interpreting dipole modeling solutions because user's interventions and decisions about the number of underlying sources are required in dipole fitting. To cope with this issue, Mosher, Lewis, and Leahy (1992) developed a mathematical approach

aimed to estimate the likely number of underlying sources. This method, called multiple signal classification (MUSIC), attempts to decompose the signal to identify underlying components in the time series data (see Mosher & Leahy, 1998 for further improvements).

In recent years, substantial progress has been made to extend the original dipole fitting approach implemented using simplified spherical head models to more realistic geometry head model constructed from single subject's MRI images, in particular using boundary element methods (BEM) or finite element methods (FEM). Not surprisingly, simulation and experimental studies have shown that a more accurate localization can be achieved by using realistic head models (e.g., Fuchs, Wagner, & Kastner, 2001). In a recent study (Cuffin, Schomer, Ives, & Blume, 2001), the best average localization that could be achieved with spherical head model was 10 mm. In addition to improved localization capability, co-registration with MRI images can be used to visualize the dipole location coordinates relative to brain anatomy, facilitating comparisons with other functional imaging modalities. Studies combining electrophysiological and hemodynamic measures have further extended dipole source localization approaches by using PET- or fMRI-identified activation loci to seed the iterative optimization procedure, providing clues about the putative location of sources (e.g., Heinze et al., 1994). As will be discussed in Section 9, the relationship between electrophysiological changes measured by EEG/MEG and hemodynamic changes measured by PET/fMRI is not fully understood (Nunez & Silberstein, 2000), posing some challenges in situations in which fMRI activations are used to choose the *number* and *location* of potential sources. A more promising (and potentially less biased) approach involves independent EEG/MEG source modeling, which is then weighted based on hemodynamic findings to select the most likely solution (e.g., Liu, Belliveau, & Dale, 1998).

In summary, although dipole source modeling has been successfully used to localize spatially restricted and focal sources (e.g., early sensory evoked potentials), its main limitation is that the *exact* number of dipoles often cannot be determined a priori. Further, because intracranial recordings have provided very little support for the notion that only a few sites in the brain are active in generating ERP or spontaneous EEG recording (e.g., Towle et al., 1998), dipole fitting results should be interpreted with caution.

8.1.1. Dipole source modeling for EEG data: FFT-dipole-approximation

As reviewed in Section 5, qEEG approaches have been extensively used in both clinical and experimental settings to investigate the spectral aspects of scalp-recorded EEG signals. For many clinical and experimental researchers, the next step following spectral analysis might be to localize the sources underlying different EEG frequency bands. Unfortunately, topographic maps of power distributions derived from traditional scalp spectral analyses cannot be used for source localization because (1) these maps represent squared potential values, in which polarity information is lost; and (b) power maps are reference-dependent (Lehmann, 1987). In 1989, Lehmann and Michel published a method, called FFT-Dipole-Approximation, which allows computation of intracerebral, three-dimensional location of single dipole source model in the frequency domain. Conceptually, this approach reduces multi-channel EEG data by focusing on the principal features of the spatial organization of brain activity. In assuming a single, common phase angle for all generator processes, the FFT-Dipole-Approximation approach models multichannel brain electric field data in the frequency domain by a potential distribution map, which contains polarity information and consequently can be used for conventional source modeling.

Analytically, standard frequency analyses via FFT are computed first. Then, for each artifact-free EEG segment, the Fourier coefficients for each electrode are plotted in a sine-cosine diagram, and subsequently projected onto the straight line given by the first principal component of the entries. Note that only assessing the first principal component of standard FFT result implies a single phase-angle modeling (i.e., all phase angles between recording electrodes are either $0°$ or $180°$), which typically explains more than 93% of the variance of the original baseline EEG data (Michel, Lehmann, Henggeler, & Brandeis, 1992). For any user-specified EEG frequency band, the single phase-angle assumption allows the computation of a mean potential distribution map (the FFT Approximation Map), which can then be subjected to standard 3-D equivalent dipole source modeling (Lehmann & Michel, 1989). In a final step, the model source's location coordinates on the anterior-posterior, left-right, and inferior-superior axes and its strength for conventional EEG frequency bands, can be compared between experimental conditions or groups.

The FFT-Dipole-Approximation method has several strengths. First, unlike scalp localization of EEG spectral value, this approach is completely independent from the chosen reference electrode location, and thus does not require any assumptions about an inactive site (Michel et al., 1992). Second, no assumption is needed about the orientation of the generating sources, thus allowing an unbiased approximation of the 3-D spatial organization of brain activity. Physiologically, locations of the model sources describe the center of gravity of all neural elements that are active in the brain during a given recording. Accordingly, different locations of centers of gravity unambiguously imply different geometry (i.e., locations and/or orientations) of the underlying neuronal sources between experimental conditions or groups. The FFT-Dipole-Approximation approach has been successfully used to compute intracerebral sources of various EEG frequency bands during experimental situations

or conditions assumed to involve widely distributed brain systems, including sleep (Tsuno et al., 2002), pathological conditions (e.g., Alzheimer's disease; Huang et al., 2000), and epilepsy (Worrell et al., 2000), among other examples. In situations, in which the assumption of a single oscillating dipole generator is unwarranted or unlikely, results are expected to be less reliable.

8.2. Linear distributed source localization techniques

Considering the intrinsic limitation of dipole modeling, and in particular the fact that it is often difficult to determine a priori the number of underlying sources, it is not surprising that attempts to develop distributed source modeling approaches have received considerable attention. In simple terms, these approaches are based on the estimation of brain electric activity at each point within a 3-D solution space. Each point, in turn, can be considered a dipole. Unlike equivalent dipole models, these "dipoles" have fixed positions (e.g., Pascual-Marqui et al., 1999) and sometimes fixed orientations (e.g., Phillips et al., 2002a; Phillips et al., 2002b), which are determined by anatomical and physiological constraints implemented within the localization algorithms. As these methods are used to estimate the strengths (and in some cases, the orientation) of the source, the equations describing distributed solutions are linear.

Because the number of measurements (electrodes) is typically <100, and the number of unknowns (electrical activity at each point in the solution space) is often in the order of 10,000, it is clear that the inverse problem is greatly underdetermined (Baillet et al., 2001; Michel et al., 2004). Mathematically, so-called regularization methods are needed to limit the range of allowable solutions and identify the "optimal" or "most likely" solution. Regularization methods can be understood as mathematical representations of the physiological/structural assumptions implemented in a given method. In the literature, various regularization methods have been utilized. Some of the most widely used include minimum norm solution (Hamalainen & Ilmoniemi, 1994), maximal smoothness (Pascual-Marqui et al., 1994), structural/functional priors (Phillips et al., 2002a; Phillips et al., 2002b), and fMRI-weighted solution space (Dale et al., 2000). Although some of these methods have received important empirical validation indicating that it is possible to solve the inverse problem, the severe underdetermined nature of the inverse problem leads to the consequence that the solutions have low spatial resolution – their solutions are often blurred. In the following section, a review of distributed source localization methods is presented. The LORETA algorithm has been used extensively by researchers in the field and by our group (e.g., Pizzagalli et al., 2001; Pizzagalli et al., 2002; Pizzagalli et al., 2003; Pizzagalli et al., 2004; Pizzagalli et al., 2006). Therefore, a more extended discussion of emerging cross-modal validation as well as limitations of LORETA will be presented in Sections 8.2.3.1 and 8.2.3.3, respectively.

8.2.1. Minimum norm solutions

The MN solution (Hamalainen & Ilmoniemi, 1994) was one of the first linear inverse solutions. In the MN approach, the head model is first mapped onto a 3-D grid, and three mutually perpendicular dipole current sources are placed at each grid point (Koles, 1998). The goal of the MN approach is to estimate the distribution and strengths of these tens of thousands of dipoles. Among the infinite possible, the MN approach selects the one that contains the least energy, that is, minimal overall current density within the brain. Mathematically, the MN solution estimates the 3-D source distribution with the smallest L2-norm solution[8] that fit the actual data.

MN does not incorporate any prior information. In particular, unlike other methods (e.g., Pascual-Marqui et al., 1994; Phillips et al., 2002a; Phillips et al., 2002b), MN solutions do not impose any spatial correlation among sources. However, there is no strong physiological evidence that the solution with the smallest L2-norm is also the most plausible one. In fact, simulation studies have shown that the MN solution typically favors weak and localized activation patterns, and can misplace deep sources onto the outermost cortex (Pascual-Marqui, 1999). Accordingly, MN does not completely fulfill the promise of a 3-D source localization technique. LORETA, as we will see, was the first approach that successfully extended the good localization properties of the 2-D MN solution to 3-D solution space.

8.2.2. Weighted minimum norm solutions

To compensate for the depth dependency of MN solution, in particular the tendency to favor superficial sources, various weighting factors have been suggested. Two solutions are mentioned here. The first, known as the *weighted MN solution*, uses a lead field normalization for compensating for the lower representation of deeper sources (e.g., Jeffs, Leahy, & Singh, 1987). The second, called FOCUSS (Focal Underdetermined System Solution; Gorodnitsky, George, & Rao, 1995), is a nonparametric algorithm for solving the inverse solution, in which the weights are iteratively modified according to the solution estimated in a previous step. Specifically, at each step, the weights of grid points with the lowest current density are reduced, and this process is repeated until the current density at most of the grid points is zero (Koles, 1998). Although these weighted MN approaches gave some promising results for reducing the low spatial resolution (blurring) of all MN solutions and for reducing the depth-dependency of sources (Michel et al., 2004), it is important to point out that weighting is selected

---

[8] In the L2-norm approach, the squared deviation of the data from a given model is minimized using a least-squares method.
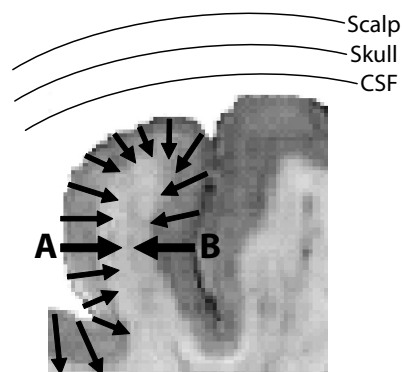
Figure 3.6. Graphical representation of the LORETA assumptions. The core assumptions of the LORETA algorithm are that (A) neighboring neurons are synchronously activated and display only gradually changing orientations; and (B) the scalp-recorded EEG originates mostly from cortical gray matter. These two assumptions are graphically displayed in the figure. Note that, in this fictive example, activity generated by the dipolar sources A and B would not be detected by scalp EEG; in fact, due to the gyral and sulcal configurations, activity from these opposing dipoles would cancel out.

based on mathematical operations rather than physiological assumptions.

8.2.3. Low-resolution Electromagnetic Tomography (LORETA)

Low-resolution Electromagnetic Tomography (LORETA) (Pascual-Marqui et al., 1994), a form of Laplacian-weighted MN solution, solves the inverse problem by assuming that: (1) neighboring neurons are synchronously activated and display only gradually changing orientations; and (2) the scalp-recorded signal originates mostly from cortical gray matter (Figure 3.6). The first assumption, which is generally consistent with neurophysiological studies in animals (e.g., Haalman & Vaadia, 1997), is mathematically implemented by computing the "smoothest" of all possible activity distributions. Note that the smoothest solution is assumed to be the most plausible one *giving rise to the scalp-recorded EEG signal*. The second assumption constrains the solution space to cortical gray matter (and hippocampi), as defined by a standard brain template. Mathematically, LORETA selects the solution with the smoothest spatial distribution by minimizing the Laplacian (i.e., the second spatial derivatives) of the current sources.

In recent implementations (Pascual-Marqui et al., 1999), LORETA uses a three-shell spherical head model registered to the Talairach brain atlas (available as digitized MRI from the Brain Imaging Centre, Montreal Neurological Institute (MNI); Evans et al., 1993) and EEG electrode coordinates derived from cross-registrations between spherical and realistic head geometry (Towle et al., 1993). The solution space, that is, the 3-D space where the inverse problem is solved, is restricted to cortical gray matter and hippocampi, as defined by a digitized

probability atlas provided by the MNI.[9] Under these constraints, the solution space includes 2394 voxels at 7 mm spatial resolution.

For analyses in the frequency domain, LORETA computes current density as the linear, weighted sum of the scalp electrical potentials, and then squares this value for each voxel to yield power of current density in units proportional to amperes per square meter (A/m^2).

In 2002, Pascual-Marqui introduced a variant of the LORETA algorithm, in which localization inferences are based on standardized current density (standardized LORETA, or sLORETA). Conceptually, sLORETA was inspired by work by Dale et al. (2000). Using a two-step process, Dale et al. first estimated current density using the MN solution; subsequently, current density was standardized using its expected standard deviation, which was assumed to fully originate from measurement noise. Although sLORETA uses a slightly different implementation that considers simultaneously two sources of variations (variations of the actual sources and variations due to noisy measurements), its localization inference is also based on standardized values of current density estimates. As a result, unlike LORETA, sLORETA does not introduce Laplacian-based spatial smoothness to solve the inverse problem and does not compute current density but rather statistical scores. In initial simulations, sLORETA was reported to have zero-localization error (Pascual-Marqui, 2002). Independent simulations using (a) a dipolar source, or (b) two spatially well-separated dipolar sources with similar depth replicated that sLORETA had higher localization accuracy than LORETA or MN solutions (Wagner, Fuchs, & Kastner, 2004). However, in the presence of a strong (or superficial) source, a second weak (or deeper) source remained undetectable by all methods, including sLORETA (Wagner et al., 2004). Thus, sLORETA successfully resolved two simultaneously active sources only when their fields were distinct enough and of similar strength.

8.2.3.1. *Cross-modal validation of LORETA.* In initial studies, the physiological validity of LORETA was indirectly evaluated by comparing LORETA solutions with functional imaging findings derived from similar experimental manipulations. For example, physiologically meaningful findings were observed during basic visual, auditory, and motor tasks (e.g., Mulert et al., 2001; Thut et al., 1999), epileptic discharges (e.g., Lantz et al., 1997), and cognitive

---

[9] Accordingly, LORETA coordinates are in MNI space. Note, however, that the LORETA software uses the Structure-Probability Maps atlas (Lancaster et al., 1997) to label gyri and Brodmann area(s). Because the MNI (used by LORETA) and the Talairach (used by the Structure-Probability Maps atlas) templates do not precisely match, MNI coordinates are temporarily converted to Talairach coordinates (Brett et al., 2002) before the Structure-Probability Maps atlas is utilized. In our publications (e.g., Pizzagalli et al., 2001, 2004) as well as those relying on the LORETA-KEY software, reported coordinates remain in MNI space.

tasks tapping specific brain regions (e.g., Pizzagalli et al., 2002).

In more recent years, important cross-modal validation has come from studies directly combining LORETA with functional fMRI (Mulert et al., 2004; Vitacco, Brandeis, Pascual-Marqui, & Martin, 2002), structural MRI (Worrell et al., 2000), PET (Pizzagalli et al., 2004; but see Gamma et al., 2004), and intracranial recordings (Seeck et al., 1998). In Pizzagalli et al. (2001), theta current density in the rostral anterior cingulate cortex (ACC) was associated with treatment response in major depression; the ACC region implicated in this 28-channel EEG study overlapped with the one implicated in similar studies using PET and fMRI (see Pizzagalli et al., 2006 for a meta-analysis). In Pizzagalli et al. (2004), subjects with the melancholic subtype of depression were characterized by decreased activity within the subgenual PFC, which was manifested as increased inhibitory EEG delta activity and decreased PET glucose metabolism (Figure 3.2A–B). Delta current density and glucose metabolism were significantly and inversely correlated ($r = -0.66$; Figure 3.2C). In two recent EEG/fMRI studies, LORETA localizations were, on average 16 mm (Mulert et al., 2004) and 14.5 mm (Vitacco et al., 2002) from fMRI activation loci, a discrepancy that is in the range of the spatial resolution of LORETA (1–2 cm). Despite some controversy in the field about the localization capability of LORETA (Grave de Peralta & Andino, 2000) and recent null findings (Gamma et al., 2004), substantial consistency between LORETA findings and other traditional neuroimaging techniques has been reported.

8.2.3.2. *Incremental validity of LORETA.* In addition to improving the spatial resolution of EEG data, initial evidence suggests that EEG source localization techniques may allow researchers to uncover information not available in traditional scalp spectral analyses. Two examples from our laboratory are pertinent to this point. In a first study, traditional scalp power and LORETA analyses were applied on the same resting EEG data to investigate putative abnormalities in major depression (Pizzagalli et al., 2002). In the LORETA data, depression severity was significantly correlated ($r = 0.60$, $p < 0.015$) with an "intracerebral" frontal asymmetry index that included the inferior and superior frontal gyri, indicating that relatively higher right prefrontal activity was associated with higher depression severity. When identical analyses were performed on the scalp frontal asymmetry index (ln F4 – ln F3), the correlation was not significant.

In a more recent study, we investigated whether resting EEG alpha activity predicted response bias in a separate verbal memory task played under different incentive (monetary) conditions (Pizzagalli, Sherwood, Henriques, & Davidson, 2005). Extending prior scalp frontal EEG asymmetry studies (e.g., Sutton and Davidson, 2000), we found that higher LORETA alpha2 (10.5–12 Hz) current
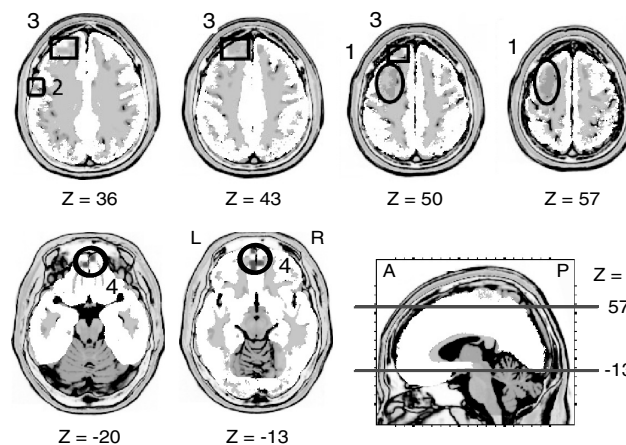

Figure 3.7. Example of LORETA findings highlighting relations between resting intracerebral EEG sources and approach-related behavior. Whole-brain analyses showing voxel-by-voxel correlations between resting alpha2 (10.5–12 Hz) current density and response bias toward reward-related cues for 18 healthy subjects. Six axial brain slices (head seen from above, nose up, L = left, R = right; A = anterior, P = posterior) are shown. Alpha2 current density within both dorsolateral prefrontal regions (clusters #1–3; see green colors) and ventromedial prefrontal regions (cluster #4; see blue colors) was negatively correlated with reward bias, indicating that higher resting activity within these regions was associated with stronger reward bias. Adapted from Pizzagalli et al. (2005).

density within left dorsolateral regions (Brodmann areas 6, 8, 9, 10, 46) was associated with stronger bias to respond to reward-related cues (Figure 3.7; see clusters #1–3). Notably, left dorsolateral prefrontal resting activity accounted for 54.8% of the variance in reward bias. Whereas this finding fits the hypothesis that frontal EEG asymmetry in favor of the left hemisphere might reflect the propensity to respond with approach-related tendencies (Davidson, 2004), a second important finding emerged: alpha2 current density within ventromedial prefrontal regions (Brodmann areas 10, 11) was also associated with reward bias (Figure 3.7; see cluster #4). This latter finding, which is consistent with functional neuroimaging and animal findings implicating the ventromedial prefrontal cortex in reward monitoring and evaluation of reinforcers, could obviously not have been achieved with scalp EEG data. More generally, findings from this study highlight that source localization techniques can be used to predict complex behavior.

8.2.3.3. *Current limitations and future directions of LORETA.* Although the LORETA algorithm has received important cross-modal validation, it is important to highlight three factors that, in most of the studies to date, likely affected the spatial resolution of this method.[10] First, the vast majority of LORETA studies have used a three-shell

---

[10] These methodological limitations are not restricted to the LORETA algorithm but would equally apply to any distributed source localization technique.

spherical head model, which represents only a rather crude approximation of the biophysical problem. As recently demonstrated by Ding, Lai, and He (2005), a more complex head model that better represents the geometry of gray and white matter regions (e.g., FEM) can substantially improve the spatial resolution of LORETA. Second, most of the studies have used a general (average) brain template (Evans et al., 1993). Clearly, use of individual anatomical MRI scans is expected to improve the precision of the solution space. Third, although LORETA studies typically used EEG electrode coordinates derived from cross-registrations between spherical and realistic head geometry (e.g., Towle et al., 1993) and registered to a MRI template, digitization of electrode positions for individual subjects is expected to further improve the spatial resolution of LORETA.

In addition to these issues, which could be addressed in the future, some more conceptual limitations should be mentioned. First, due to the smoothness assumption used to solve the inverse problem, LORETA is incapable of resolving activity from closely spaced sources; in such cases, LORETA will find a smeared, single source located between the original two sources. In fact, in experimental situations in which the generating source is known to be well-represented by a single dipole (e.g., early sensory ERPs), dipole fitting procedures might be preferred, as LORETA will tend to blur the solution (e.g., Fuchs, Wagner, Kohler, & Wischmann, 1999; Moffitt & Grill, 2004). Moreover, despite the fact that LORETA showed the smallest overall localization error in the simulations by Fuchs et al. (1999), these authors found that LORETA tended to overestimate the depth of sources at eccentricities above 70%, likely due to the fact that the 3-D smoothness constraint is difficult to fulfill at the boundary of the solution space. Second, some authors have argued that the electrophysiological and neuroanatomical constrains used by LORETA are somewhat arbitrary. In particular, concerns have been raised about whether the assumption of maximal synchronization between neighboring neuronal populations can be appropriately extended to adjacent voxels (Kincses, Braun, Kaiser, & Elbert, 1999). Third, although sources in LORETA are appropriately constrained to gray matter, their orientation is left undetermined. Phillips et al. (2002a,b) have recently shown that EEG distributed source localization approaches can make better use of anatomical constraints. For example, in their approach, dipole orientation was fixed perpendicular to the interface between gray and white matter, as derived from high-resolution MRI. Fourth, at least in current implementations, LORETA does not accommodate other functional priors (e.g., weighting factors based on independently assessed fMRI activations), which have been recently used to limit the spatial dispersion of distributed source localization techniques (e.g., Phillips et al., 2002a; Phillips et al., 2002b; Dale et al., 2000). Success in addressing these issues is expected to further improve the LORETA localization accuracy.

8.2.4. Variable resolution electromagnetic tomography (VARETA)

Frequency-domain VARETA is a discrete, spline distributed solution[11] that has been used to estimate sources of EEG frequency bands (Valdes-Sosa, Marti, Garcia, & Casanova, 1996; Bosch-Bayard et al., 2001). Conceptually, it belongs to the family of weighted MN solutions.

As mentioned above, LORETA imposes maximal spatial smoothness; as a consequence, LORETA is able to recover smoothly distributed sources with low localization error, but focal sources are blurred. VARETA, on the other hand, utilizes different amounts of spatial smoothness for different types of generators. This is achieved by a data-driven procedure that estimates the spatial covariance matrix through the scalp cross-spectra, which ultimately selects the amount of spatial smoothness required at each voxel in the brain (Valdes-Sosa et al., 1996). Mathematically, this is done by allowing the regularization parameter to vary according to the location in the solution space. According to the developers, a further key difference between LORETA and their algorithm is that VARETA is able to estimate discrete and distributed sources with equal accuracy (Fernandez-Bouzas et al., 1999). Nonetheless, initial empirical findings seem to contain substantial degree of blurring (e.g., Fernandez et al., 2000; Bosch-Bayard et al., 2001).

In VARETA, current sources are also restricted to gray matter, as defined by a probabilistic brain atlas. Currently, a limited number of studies have used VARETA, although encouraging results have been reported for localizing EEG current density during normative mental processes (e.g., Fernandez et al., 2000) as well as in pathological conditions (e.g., Fernandez-Bouzas et al., 1999). Additional testing from independent laboratories will be important to assess the validity of this promising approach.

8.2.5. Local Auto-Regressive Average (LAURA)

In 2001, Grave de Peralta and colleagues (Grave de Peralta et al., 2001) proposed a distributed linear inverse solution that constrains the minimum norm solution based on biophysical laws. To solve the inverse problem, this technique selects the source configuration that better mirrors the biophysical behavior of electric vector fields. Mathematically, this approach uses a Local Auto-Regressive Average (LAURA) model with coefficients that depend on the distances between solution points in order to mirror the electromagnetic laws that (a) the strength of the source declines with the inverse of the squared distance of the potential field; and (b) the estimated activity at one point depends on the activity at neighboring points. As with other distributed inverse solutions, this method makes no assumptions about the number or location of active sources. Simulation studies show that LAURA is able to resolve multiple simultaneously active sources (Grave de

---

[11] Spline estimates can be understood as the spatially smoothest solutions accounting for the observed data.

Peralta et al., 2001), and promising applications have recently appeared (e.g., Murray et al., 2004).

8.2.6. Bayesian solutions

In recent years, Bayesian approaches have attracted increased attention because they allow incorporation of a priori information into source estimation by means of probability distributions (Phillips et al., 2002a; Phillips et al., 2002b; Trujillo-Barreto et al., 2004). For example, Phillips et al. (2002a,b) described an EEG source localization approach based on the weighted MN solution that incorporates physiological and anatomical constraints derived from other imaging modalities. Their approach rests on three anatomical/physiological assumptions, which are used to reduce the solution space a priori. They assume that sources are: (1) located in gray matter; (2) oriented perpendicularly to the cortical mantle; and (3) locally coherent (i.e., their activity changes smoothly along the cortical mantle). The first assumption can be implemented by constraining the solution space to gray matter, as determined by single subject's structural MRI (e.g., Phillips et al., 2002a). This step can be achieved by segmenting an MRI image into gray matter, white matter, and cerebrospinal fluid and creating a mask containing a gray matter coefficient value ranging from 0 (null probability that a given voxel is in gray matter) to 1 (100% probability). Anatomical information gathered in this first step can also be used to constrain the orientation of a local dipole to fulfill the requirements of the second assumption. Although a description of the mathematical corollaries of these assumptions is beyond the scope of this chapter, it is clear that by determining a priori the orientation of dipoles based on well-grounded anatomical and physiological bases, the inverse problem is reduced from a vectorial problem (orientation and strength are unknown) to a scalar problem (only strength is unknown). The third assumption of locally coherent and synchronized electrical activity can be met by imposing spatial smoothness (Pascual-Marqui et al., 1994), which is mathematically implemented by minimizing differences among neighboring voxels.

In addition to these assumptions, which are essentially identical to the ones implemented by LORETA, Phillips et al. (2002b)'s method allows the use of basis functions to further reduce the solution space in the temporal and spatial domains; in the spatial domain, weighting factors can be introduced a priori based on independent information derived from fMRI, for example. Simulations showed that (1) in the absence of noise and localization priors, the best localization was achieved with a relatively large smoothness constraint; and (2) location priors greatly improved the localization accuracy, even in the presence of noise and with reduced smoothing.

In a recent extension of the Bayesian approach, Trujillo-Barreto et al. (2004) proposed a technique that calculates a "final" solution through averaging of various models, each with different anatomical constraints, which are weighted based on their probability of contributing to the generation of EEG signals. In initial evaluations with simulated and real EEG data, this approach has shown promising findings (Trujillo-Barreto et al., 2004).

8.2.7. Simulation studies comparing different distributed inverse solutions

As evident from the previous section, the past decade has witnessed substantial progress in developing distributed source localization techniques that do not assume a priori the number and location of underlying sources. Although these approaches have similarities and an identical goal (i.e., to solve the underdetermined and ill-posed inverse problem), they often differ in the nature and extent of the anatomical, physiological, and/or statistical assumptions they implement. Ultimately, no matter how sophisticated their mathematical and biophysical implementations are, the validity and reliability of *any* of these methods should be exclusively evaluated by their ability to provide physiologically meaningful solutions, in particular in relations to other neuroimaging techniques (e.g., fMRI, PET; but see Section 9 for a discussion of challenges relating electrophysiological and hemodynamic measures).

For most of these techniques, however, their reliability and validity have been evaluated by means of artificial data. In these simulation studies, four basic steps are used (Michel et al., 2004): (1) dipole(s) is/are placed at each grid of the solution space; (2) the forward solution is computed to determine the associated scalp potential distribution; (3) sources underlying the scalp potential distribution are estimated using various source localization techniques; and (4) a localization error is computed by comparing the initial and estimated source location. Over the years, several simulations have been published, and a brief summary is reported in the following section.

Pascual-Marqui (1999) compared LORETA, MN, weighted MN, and other linear, distributed inverse solutions. He reported that only LORETA was capable of correct localization with, on average, localization error of 1 voxel resolution, whereas the other methods showed large localization errors, in particular with deep sources. Although LORETA showed the best 3-D localization accuracy, it is important to stress that LORETA tended to underestimate deep sources and that correct localization was achieved with some degree of blurring. Higher localization accuracy for LORETA compared to standard MN solutions has also been reported by Fuchs et al. (1999) and Babiloni et al. (2004a). Fuchs et al. (1999)'s simulations showed, however, that the MN tended to emphasize superficial sources, whereas LORETA tended to suppress them, yielding instead overly deep, blurred solutions for the same sources. In a later simulation, Pascual-Marqui et al. (2002) compared the localization error and spatial dispersion (i.e., resolution) of sLORETA, MN (Hamalainen & Ilmoniemi, 1994), and a new tomographic method described by Dale et al. (2000). Findings showed that sLORETA had smaller localization error and

higher spatial resolution, irrespective of the presence or absence of noise and source orientation. Indeed, sLORETA was the only algorithm achieving zero-error localization. Moreover, the spatial blurring of sLORETA was smaller than the one achieved by the method employed by Dale et al. (2000). Recently, Yao and Dewald (2005) compared the performance of moving dipoles, MN solution, and LORETA using simulated EEG data and real ERP data. Compared to the other methods, LORETA had the smallest localization error, as well as the smallest percentage of undetected sources and falsely-detected sources in simulated EEG data. Not unexpectedly, LORETA (as well as the other methods) was unable to separate two discrete sources spaced only by 5 mm. Whereas these simulation studies used the three-spherical head model to solve the inverse solution, Ding et al. (2005) recently evaluated the localization accuracy of LORETA using a realistic geometry head model (BEM). As expected, the LORETA localization error was lower when using the BEM compared to the spherical head model (approximately 10 mm vs. 20–30 mm).

Other simulations, however, have challenged the localization accuracy of LORETA. Grave de Peralta et al. (2001), for example, compared MN, weighted MN, LORETA, and LAURA, and found the best localization accuracy for LAURA, followed by LORETA and the weighted MN solution, which showed similar performances. Similarly, Trujillo-Barreto et al. (2004) compared LORETA with an extension of the Bayesian model incorporating probabilistic maps derived from segmentation of standard brain template within 71 separate brain regions, and found that the latter method gave higher localization accuracy and less spatial distortion (i.e., higher spatial resolution), particularly when subcortical regions were implicated. Better localization accuracy of a Bayesian model incorporating structural and physiological priors compared to LORETA was also reported by Phillips et al. (2002a,b). Indeed, in their simulations, Phillips et al. (2002a,b) showed that the inclusion of a priori location information improved the performance of the distributed minimum norm approach, whereas LORETA tended to oversmooth the solution. In the absence of prior information about location, Phillips's method and LORETA achieved similar localization capabilities.

As correctly pointed out by Michel et al. (2004), these simulation studies are intrinsically limited by the fact that the dipole localization error used to evaluate the "goodness" of any distributed inverse solution is the "most unnatural test for them." In fact, as mentioned above, distributed source localization techniques have been developed to resolve multiple and spatially distributed sources, and thus these simulations cannot predict "how a distributed inverse solution deals with the reciprocal influences of simultaneously active sources (Michel et al., 2004; p. 2205)." Accordingly, real EEG data collected during functionally and anatomically well-characterized experimental tasks (e.g., finger tapping, checkerboard stimula-

tion, N-back working memory task) may provide a better test of various source localization algorithms. Additionally, physiological validation through other neuroimaging techniques would provide converging evidence. As reviewed in Section 4.3.1., encouraging cross-modal validity has started to emerge for the LORETA algorithm, particularly in studies comparing LORETA with functional fMRI (Mulert et al., 2004; Vitacco et al., 2002), structural MRI (Worrell et al., 2000), PET (Pizzagalli et al., 2004), and intracranial recordings (Seeck et al., 1998). Similar cross-modal validity will be necessary for evaluating the localization accuracy of other distributed source localization techniques.

8.2.8. The issue of multiple testing

As with hemodynamic neuroimaging studies, which typically involve statistical comparisons at thousands or tens of thousands of locations in the brain, distributed EEG source localization techniques also face the issue of how best to determine a statistical threshold that will protect against Type I errors due to multiple comparisons. In our own work with LORETA (e.g., Pizzagalli et al., 2001), we have implemented a randomization procedure based on the t_{max} approach to estimate the false-positive rate under the Null Hypothesis of no voxel-wise differences between two given groups or conditions. This approach, which was inspired by statistical solutions developed for neuroimaging data (Arndt et al., 1996; Holmes et al., 1996), relies on permutation procedures. When comparing an experimental and a control group, for example, two randomly selected groups each containing half of the subjects under investigation can be tested at each of the 2394 voxels. At every iteration, the largest absolute t value (from a two-tailed test) can then be stored in a histogram. After 5000 iterations, the t value cutting off the most extreme 5% of the distribution can be identified and used to threshold the data, i.e., to accept or reject the Null Hypothesis.

8.2.9. Summary

The main goal of *any* EEG source imaging technique is to draw reliable conclusions about sources underlying scalp-recorded signals, that is, to solve the inverse problem. Importantly, the choice of the inverse method also depends on the experimental situation. Dipole fitting methods can provide accurate localization in situations of highly focal activations, for example during somatosensory stimulation or epileptic discharges (Michel et al., 2004; Fuchs et al., 2004). In more complex cognitive or pathological conditions that likely recruit widespread neuronal networks, distributed imaging techniques are expected to perform better.

As appropriately emphasized by Michel et al. (2004), it should be beyond the scope of any review to declare a specific source localization algorithm as "the best". Two main reasons justify this position. First, as discussed above, simulation studies based on focal sources may not be

the most appropriate test of the localization accuracy of distributed source localization techniques, which may perform substantially better when real EEG data generated by widely distributed neuronal networks are considered. Second, inconsistencies and even contradictions between simulation studies stemming from different laboratories raise some concerns about (1) the mathematical implementations of "competing" localization algorithm (e.g., Pascual-Marqui et al., 2002 for a discussion of this important point); and (2) the selection of test sources that might favor a given algorithms over the others. Clearly, in order to progress in this important field, independent validation studies devoid of experimenter bias or preferences are needed.

9. DIFFICULTIES INTEGRATING ELECTROMAGNETIC AND HEMODYNAMIC VARIABLES

Approaches integrating EEG and PET/fMRI are based on the assumption that brain regions that are electrically more active over time will also show increases in metabolic or hemodynamic activities. Although this assumption is plausible (Logothetis, Pauls, Augath, Trinath, & Oeltermann, 2001), several factors contribute to a difficult comparison between electrophysiological and hemodynamic techniques, making a complete integration conceptually challenging (Nunez & Silberstein, 2000). First, due to the fundamentally different physiological basis of electromagnetic and hemodynamic measures, situations can arise in which the activation period of neurons is too brief to produce a detectable hemodynamic change, whereas it could be easily detected by EEG. Second, scalp EEG signals are highly dependent on synchronization/desynchronization mechanisms, and their relation to glucose or oxygen utilization is unclear (Nunez & Silberstein, 2000). For example, increased neuronal firing and reduced synchrony would produce a small scalp EEG (e.g., alpha blockade after eye opening), a process that would require, however, substantial metabolic supply. Similarly, based on the observation that both excitatory and inhibitory processes require glucose utilization (Ackermann, Finch, Babb, & Engel, 1984), loss of inhibitory synaptic action in pathological conditions (e.g., interictal periods in epileptic patients) would produce large EEG signals but decreased PET metabolic signal. Third, whereas hemodynamic measures are not affected by the spatial arrangement of the activated neurons, scalp EEG cannot detect activity from neuronal assemblies arranged in closed electrical fields (Nunez & Silberstein, 2000). This may explain why in the EEG literature it has been generally very difficult to reliably measure sources originating from the hippocampus, which represents a closed field due to its structural features. Along similar lines, spatial configurations of sources involving opposing dipoles located in sulci would generate activity that cannot be detected by scalp EEG, as the opposing dipoles would cancel (see dipolar sources A and B in Figure 3.6).

Consistent with these fundamental limitations, empirical evidence indicates that integration of electromagnetic and hemodynamic measures works extremely well in situations in which the fMRI and EEG/MEG activations correspond (Dale et al., 2000). However, in cases of imperfect or lacking correspondence between the fMRI and MEG/EEG activations, erroneous findings are likely to emerge (Baillet et al., 2001).

10. CONCLUSIONS

The past 20 years have witnessed unprecedented progress in our ability to study human brain function noninvasively. The high temporal resolution of electromagnetic measurements (EEG/MEG) continues to offer a unique window into the dynamics of brain function. In particular, EEG/MEG measures are exquisitely sensitive to spontaneous and induced changes of the functional brain state allowing investigation of brain mechanisms associated with covert internal states, which may not necessarily be accessible to introspection or behavioral observation.

The field of EEG research has perhaps witnessed its largest advances in the critical area of source imaging. A variety of innovative and sophisticated solutions for estimating intracerebral sources are continuing to emerge. In particular, approaches that make no a priori assumptions about the number of underlying sources and incorporate physiologically and anatomically sound priors to mathematically constrain the inverse solution have shown promising results. These improvements have opened exciting new avenues for functional brain imaging with both high temporal and spatial resolution. This is especially relevant for the wide range of experimental situations in which distributed neural networks are implicated.

In conclusion, advances in spatial sampling through high-density recordings, development of more realistic head models through high-resolution MRI, substantial progress in source localization techniques, and integration of different functional neuroimaging techniques have all contributed to improving our ability to investigate spatiotemporal dynamics of brain mechanisms underlying normal and pathological mental processes and states. In fact, the picture emerging from these methodological and conceptual improvements is that the spatial resolution of the EEG may approach that of other neuroimaging approaches, particularly when spatially smoothed fMRI or PET data are considered (e.g., Michel et al., 2004; Babiloni et al., 2004b). In the years to come, critical contributions to our understanding of the human mind can be expected from the EEG field.

REFERENCES

Ackermann, R. F., Finch, D. M., Babb, T. L., & Engel, J., Jr. (1984). Increased glucose metabolism during long-duration recurrent inhibition of hippocampal pyramidal cells. *Journal of Neuroscience, 4,* 251–264.

Allen, J. J. B., Coan, J. A., & Nazarian, M. (2004) Issues and assumptions on the road from raw signals to metrics of frontal EEG asymmetry in emotion. *Biological Psychology, 67,* 183–218.

American Electroencephalographic Society (1991). Guidelines for standard electrode position nomenclature. *Journal of Clinical Neurophysiology, 8,* 200–202.

Ary, J. P., Klein, S. A., & Fender, D. H. (1981). Location of sources of evoked scalp potentials: corrections for skull and scalp thickness. *IEEE Transactions on Biomedical Engineering, 28,* 447–452.

Arndt, S., Cizadlo, T., Andreasen, N. C., Heckel, D., Gold, S., O'Leary, D. S. (1996). Tests for comparing images based on randomization and permutation methods. *Journal of Cerebral Blood Flow & Metabolism, 16,* 1271–1279.

Asada, H., Fukuda, Y., Tsunoda, S., Yamaguchi, M., & Tonoike, M. (1999). Frontal midline theta rhythms reflect alternative activation of prefrontal cortex and anterior cingulate cortex in humans. *Neuroscience Letters, 274,* 29–32.

Astolfi, L., Cincotti, F., Mattia, D., Babiloni, C., Carducci, F., Basilisco, A. et al. (2005). Assessing cortical functional connectivity by linear inverse estimation and directed transfer function: simulations and application to real data. *Clinical Neurophysiology, 116,* 920–932.

Babiloni, F., Babiloni, C., Carducci, F., Fattorini, L., Onorati, P., & Urbano, A. (1996). Spline Laplacian estimate of EEG potentials over a realistic magnetic resonance-constructed scalp surface model. *Electroencephalography and Clinical Neurophysiology, 98,* 363–373.

Babiloni, F., Babiloni, C., Carducci, F., Romani, G. L., Rossini, P. M., Angelone, L. M., Cincotti, F. (2004a). Multimodal integration of EEG and MEG data: a simulation study with variable signal-to-noise ratio and number of sensors. *Human Brain Mapping, 22,* 52–62.

Babiloni, F., Mattia, D., Babiloni, C., Astolfi, L., Salinari, S., Basilisco, A. et al. (2004b). Multimodal integration of EEG, MEG and fMRI data for the solution of the neuroimage puzzle. *Magnetic Resonance Imaging, 22,* 1471–1476.

Baillet, S., Mosher, J. C., & Leahy, R. M. (2001). Electromagnetic Brain Mapping. *IEEE Signal Processing Magazine, 18,* 14–30.

Berger, H. (1929). Uber das Elektrenkephalogramm des Menschen. *Archiv für Psychiatrie und Nervenkrankheit, 87,* 555–574.

Bland, B. H. & Oddie, S. D. (1998). Anatomical, electrophysiological and pharmacological studies of ascending brainstem hippocampal synchronizing pathways. *Neuroscience and Biobehavioral Reviews, 22,* 259–273.

Borst, J. G., Leung, L. W., & MacFabe, D. F. (1987). Electrical activity of the cingulate cortex. II. Cholinergic modulation. *Brain Research, 407,* 81–93.

Bosch-Bayard, J., Valdes-Sosa, P., Virues-Alba, T., Aubert-Vazquez, E., John, E. R., Harmony, T. et al. (2001). 3D statistical parametric mapping of EEG source spectra by means of variable resolution electromagnetic tomography (VARETA). *Clinical Electroencephalography, 32,* 47–61.

Bouyer, J. J., Montaron, M. F., Vahnee, J. M., Albert, M. P., & Rougeul, A. (1987). Anatomical localization of cortical beta rhythms in cat. *Neuroscience, 22,* 863–869.

Bressler, S. L. & Kelso, J. A. (2001). Cortical coordination dynamics and cognition. *Trends in Cognitive Sciences, 5,* 26–36.

Brett, M., Johnsrude, I. S., & Owen, A. M. (2002). The problem of functional localization in the human brain. *Nature Review Neuroscience, 3,* 243–249.

Buzsaki, G. (1996). The hippocampo-neocortical dialogue. *Cerebral Cortex, 6,* 81–92.

Buzsaki, G. & Draguhn, A. (2004). Neuronal oscillations in cortical networks. *Science, 304, 1926–1929.*

Cantero, J. L., Atienza, M., Salas, R. M., & Gomez, C. M. (1999). Brain spatial microstates of human spontaneous alpha activity in relaxed wakefulness, drowsiness period, and REM sleep. *Brain Topography, 11,* 257–263.

Coan, J. A. & Allen, J. J. B. (2004). Frontal EEG asymmetry as a moderator and mediator of emotion. *Biological Psychology, 67,* 7–50.

Cooper, N. R., Croft, R. J., Dominey, S. J., Burgess, A. P., & Gruzelier, J. H. (2003). Paradox lost? Exploring the role of alpha oscillations during externally vs. internally directed attention and the implications for idling and inhibition hypotheses. *International Journal of Psychophysiology, 47,* 65–74.

Coutin-Churchman, P., Anez, Y., Uzcategui, M., Alvarez, L., Vergara, F., Mendez, L. et al. (2003). Quantitative spectral analysis of EEG in psychiatry revisited: drawing signs out of numbers in a clinical setting. *Clinical Neurophysiology, 114,* 2294–2306.

Croft, R. J., Chandler, J. S., Barry, R. J., Cooper, N. R., & Clarke, A. R. (2005). EOG correction: a comparison of four methods. *Psychophysiology, 42,* 16–24.

Cuffin, B. N., Schomer, D. L., Ives, J. R., & Blume, H. (2001). Experimental tests of EEG source localization accuracy in spherical head models. *Clinical Neurophysiology, 112,* 46–51.

Dale, A. M., Liu, A. K., Fischl, B. R., Buckner, R. L., Belliveau, J. W., Lewine, J. D. et al. (2000). Dynamic statistical parametric mapping: combining fMRI and MEG for high-resolution imaging of cortical activity. *Neuron, 26,* 55–67.

Davidson, R. J., Jackson, D. C., & Larson, C. L. (2000). Human Electroencephalography. In J.T. Cacioppo, L. G. Tassinary, & G. G. Bernston (Eds.), Handbook of Psychophysiology (2nd ed., pp. 27–56). Cambridge: Cambridge University Press.

Dien, J. (1998). Issues in the application of the average reference: Review, critiques, and recommendations. *Behavioral Research Methods, Instruments, and Computers, 30,* 34–43.

Ding, L., Lai, Y., & He, B. (2005). Low resolution brain electromagnetic tomography in a realistic geometry head model: a simulation study. *Physics in Medicine and Biology, 50,* 45–56.

Duffy, F. H., Burchfiel, J. L., & Lombroso, C. T. (1979). Brain electrical activity mapping (BEAM): a method for extending the clinical utility of EEG and evoked potential data. *Annals of Neurology, 5,* 309–321.

Dumermuth, G. & Molinari, L. (1987). Spectral analysis of EEG background activity. In A.S. Gevins & A. Remond (Eds.), *Handbook of Electroencephalography and Clinical Neurophysiology: Methods of Analysis of Brain Electrical and Magnetic Signals* (Revised Series ed., pp. 85–125). Amsterdam: Elsevier.

Engel, A. K., Fries, P., & Singer, W. (2001). Dynamic predictions: oscillations and synchrony in top-down processing. *Nature Reviews Neuroscience, 2,* 704–716.

Evans, A. C., Collins, D. L., Mills, S. R., Brown, E. D., Kelly, R. L., & Peters, T. M. (1993). 3D statistical neuroanatomical models from 305 MRI volumes. *Proceedings IEEE Nuclear Science Symposium and Medical Imaging Conference, 95,* 1813–1817.

Fell, J., Klaver, P., Elfadil, H., Schaller, C., Elger, C. E., & Fernandez, G. (2003). Rhinal-hippocampal theta coherence during declarative memory formation: Interaction with gamma synchronization? *European Journal of Neuroscience, 17,* 1082–1088.

Fender, D. H. (1987). Source localization of brain electrical activity. In A.S. Gevins & A. Remond (Eds.), *Methods of Analysis of Brain Electrical and Magnetic Signals* (pp. 355–403). Amsterdam; New York; Oxford: Elsevier.

Fernandez, T., Harmony, T., Silva-Pereyra, J., Fernandez-Bouzas, A., Gersenowies, J., Galan, L. et al. (2000). Specific EEG frequencies at specific brain areas and performance. *Neuroreport, 11,* 2663–2668.

Fernandez-Bouzas, A., Harmony, T., Bosch, J., Aubert, E., Fernandez, T., Valdes, P. et al. (1999). Sources of abnormal EEG activity in the presence of brain lesions. *Clinical Electroencephalography, 30,* 46–52.

Fink, A., Grabner, R. H., Neuper, C., & Neubauer, A. C. (2005). EEG alpha band dissociation with increasing task demands. *Cognitive Brain Research, 24,* 252–259.

Fisch, B. J. (1999). *Fisch & Spehlmann's EEG Primer: Basic Principles of Digital and Analog EEG.* (3rd (revised) ed.) Amsterdam: Elsevier.

Fuchs, M., Ford, M. R., Sands, S., & Lew, H. L. (2004). Overview of dipole source localization. *Physical Medicine and Rehabilitation Clinics of North America., 15,* 251–262.

Fuchs, M., Wagner, M., & Kastner, J. (2001). Boundary element method volume conductor models for EEG source reconstruction. *Clinical Neurophysiology, 112,* 1400–1407.

Fuchs, M., Wagner, M., Kohler, T., & Wischmann, H. A. (1999). Linear and nonlinear current density reconstructions. *Journal of Clinical Neurophysiology, 16,* 267–295.

Gamma, A., Lehmann, D., Frei, E., Iwata, K., Pascual-Marqui, R. D., & Vollenweider, F. X. (2004). Comparison of simultaneously recorded [H2(15)O]-PET and LORETA during cognitive and pharmacological activation. *Human Brain Mapping, 22,* 83–96.

Gasser, T. & Molinari, L. (1996). The analysis of the EEG. *Statistical Methods in Medical Research, 5,* 67–99.

Gevins, A., Le, J., Martin, N. K., Brickett, P., Desmond, J., & Reutter, B. (1994). High resolution EEG: 124-channel recording, spatial deblurring and MRI integration methods. *Electroencephalography & Clinical Neurophysiology, 90,* 337–358.

Gilmore, P. C. & Brenner, R. P. (1981). Correlation of EEG, computerized tomography, and clinical findings. Study of 100 patients with focal delta activity. *Archives of Neurology, 38,* 371–372.

Gorodnitsky, I. F., George, J. S., & Rao, B. D. (1995). Neuromagnetic source imaging with FOCUSS: a recursive weighted minimum norm algorithm. *Electroencephalography & Clinical Neurophysiology, 95,* 231–251.

Grave de Peralta Menendez R. & Gonzalez Andino, S. L. (2000). Discussing the Capabilities of Laplacian Minimization. *Brain Topography, 13,* 97–104.

Grave de Peralta, M. R., Gonzalez, A. S., Lantz, G., Michel, C. M., & Landis, T. (2001). Noninvasive localization of electromagnetic epileptic activity. I. Method descriptions and simulations. *Brain Topography, 14,* 131–137.

Greischar, L. L., Burghy, C. A., van Reekum, C. M., Jackson, D. C., Pizzagalli, D. A., Mueller, C. et al. (2004). Effects of electrode density and electrolyte spreading in dense array electroencephalographic recording. *Clinical Neurophysiology, 115,* 710–720.

Gross, D. W. & Gotman, J. (1999). Correlation of high-frequency oscillations with the sleep-wake cycle and cognitive activity in humans. *Neuroscience, 94,* 1005–1018.

Haalman, I. & Vaadia, E. (1997). Dynamics of neuronal interactions: Relation to behavior, firing rates, and distance between neurons. *Human Brain Mapping, 5,* 249–253.

Hagemann, D., & Naumann, E. (2001). The effects of ocular artifacts on (lateralized) broadband power in the EEG. *Clinical Neurophysiology, 112,* 215–231.

Hamalainen, M. S. & Ilmoniemi, R. J. (1994). Interpreting magnetic fields of the brain: minimum norm estimates. *Medical & Biological Engineering & Computing, 32,* 35–42.

Hamalainen, M. S. & Sarvas, J. (1989). Realistic conductivity geometry model of the human head for interpretation of neuromagnetic data. *IEEE Transactions on Biomedical Engineering, 36,* 165–171.

He, B. (1999). Brain electric source imaging: Scalp Laplacian mapping and cortical imaging. *Critical Reviews in Biomedical Engineering, 27,* 149–188.

Heinze, H. J., Mangun, G. R., Burchert, W., Hinrichs, H., Scholz, M., Munte, T. F. et al. (1994). Combined spatial and temporal imaging of brain activity during visual selective attention in humans. *Nature, 372,* 543–546.

Helmholtz, H. L. F. (1853). Ueber einige Gesetze der Vertheilung elektrischer Ströme in körperlichen Leitern mit Anwendung aud die thierisch-elektrischen Versuche. *Annalen der Physik und Chemie, 9,* 211–233.

Hjorth, B. (1975). An on-line transformation of EEG scalp potentials into orthogonal source derivations. *Electroencephalography & Clinical Neurophysiology, 39,* 526–530.

Holmes, A. P., Blair, R. C., Watson, J. D. G, & Ford, I (1996). Nonparametric analysis of statistic images from functional mapping experiments. *Journal of Cerebral Blood Flow & Metabolism, 16,* 7–22.

Huang, C., Wahlund, L., Dierks, T., Julin, P., Winblad, B., & Jelic, V. (2000). Discrimination of Alzheimer's disease and mild cognitive impairment by equivalent EEG sources: a cross-sectional and longitudinal study. *Clinical Neurophysiology, 111,* 1961–1967.

Hughes, J. R. & John, E. R. (1999). Conventional and quantitative electroencephalography in psychiatry. *Journal of Neuropsychiatry and Clinical Neurosciences, 11,* 190–208.

Jasper, H. H. (1958). The ten-twenty electrode system of the International Federation. *Electroencephalography & Clinical Neurophysiology, 10,* 371–375.

Jeffs, B., Leahy, R., & Singh, M. (1987). An evaluation of methods for neuromagnetic image reconstruction. *IEEE Transactions on Biomedical Engineering, 34,* 713–723.

John, E. R., Ahn, H., Prichep, L., Trepetin, M., Brown, D., & Kaye, H. (1980). Developmental equations for the electroencephalogram. *Science, 210,* 1255–1258.

Kincses, W. E., Braun, C., Kaiser, S., & Elbert, T. (1999). Modeling extended sources of event-related potentials using anatomical and physiological constraints. *Human Brain Mapping, 8,* 182–193.

Klimesch, W. (1999). EEG alpha and theta oscillations reflect cognitive and memory performance: A review and analysis. *Brain Research Reviews, 29,* 169–195.

Koenig, T., Prichep, L., Lehmann, D., Sosa, P. V., Braeker, E., Kleinlogel, H. et al. (2002). Millisecond by millisecond, year by year: normative EEG microstates and developmental stages. *Neuroimage, 16,* 41–48.

Koles, Z. J. (1998). Trends in EEG source localization. *Electroencephalography & Clinical Neurophysiology, 106,* 127–137.

Lancaster, J. L., Rainey, L. H., Summerlin, J. L., Freitas, C. S., Fox, P. T., Evans, A. C., et al. Automated labeling of the human brain: A preliminary report on the development and evaluation of a forward-transformed method. *Human Brain Mapping, 5,* 238–242.

Lantz, G., Grave de Peralta, R., Spinelli, L., Seeck, M., & Michel, C. M. (2003). Epileptic source localization with high density EEG: how many electrodes are needed? *Clinical Neurophysiology, 114,* 63–69.

Lantz, G., Michel, C. M., Pascual-Marqui, R. D., Spinelli, L., Seeck, M., Seri, S., et al. (1997). Extracranial localization of intracranial interictal epileptiform activity using LORETA (low resolution electromagnetic tomography). *Electroencephalography & Clinical Neurophysiology, 102,* 414–422.

Larson, C. L., Davidson, R. J., Abercrombie, H. C., Ward, R. T., Schaefer, S. M., Jackson, D. C., Holden, J. E., & Perlman, S. B. (1998). Relations between PET-derived measures of thalamic glucose metabolism and EEG alpha power. *Psychophysiology, 35,* 162–169.

Lehmann, D. (1971). Multichannel topography of human alpha EEG fields. *Electroencephalography & Clinical Neurophysiology, 31,* 439–449.

Lehmann, D. (1990). Brain electric microstates and cognition: The atoms of thought. In E.R. John (Ed.), *Machinery of the Mind.* Boston: Birkhäuser, pp. 209–224.

Lehmann, D. (1987). Principles of spatial analysis. In A.S. Gevins & A. Remond (Eds.), *Handbook of Electroencephalography and Clinical Neurophysiology: Methods of Analysis of Brain Electrical and Magnetic Signals* (Revised Series ed., pp. 309–354). Amsterdam: Elsevier.

Lehmann, D., Faber, P. L., Galderisi, S., Herrmann, W. M., Kinoshita, T., Koukkou, M. et al. (2005). EEG microstate duration and syntax in acute, medication-naive, first-episode schizophrenia: a multi-center study. *Psychiatry Research, 138,* 141–156.

Lehmann, D., Henggeler, B., Koukkou, M., & Michel, C. M. (1993). Source localization of brain electric field frequency bands during conscious, spontaneous, visual imagery and abstract thought. *Brain Research: Cognitive Brain Research, 1,* 203–210.

Lehmann, D. & Michel, C. M. (1989). Intracerebral dipole sources of EEG FFT power maps. *Brain Topography, 2,* 155–164.

Leoncani, L. & Comi, G. (1999). EEG coherence in pathological conditions. *Journal of Clinical Neurophysiology, 16,* 548–555.

Liu, A. K., Belliveau, J. W., & Dale, A. M. (1998). Spatiotemporal imaging of human brain activity using functional MRI constrained magnetoencephalography data: Monte Carlo simulations. *Proceedings of National Sciences of the United States of America, 95,* 8945–8950.

Llinas, R. R. (1988). The intrinsic electrophysiological properties of mammalian neurons: insights into central nervous system function. *Science, 242,* 1654–1664.

Llinas, R. R., Ribary, U., Jeanmonod, D., Kronberg, E., & Mitra, P. P. (1999). Thalamocortical dysrhythmia: A neurological and neuropsychiatric syndrome characterized by magnetoencephalography. *Proceedings of the National Academy of Sciences of the United States of America, 96,* 15222–15227.

Logothetis, N. K., Pauls, J., Augath, M., Trinath, T., & Oeltermann, A. (2001). Neurophysiological investigation of the basis of the fMRI signal. *Nature, 412,* 150–157.

Lopes da Silva, F. (2004). Functional localization of brain sources using EEG and/or MEG data: volume conductor and source models. *Magnetic Resonance Imaging, 22,* 1533–1538.

Luu, P., Tucker, D. M., Derryberry, D., Reed, M., & Poulsen, C. (2003). Electrophysiological responses to errors and feedback in the process of action regulation. *Psychological Science, 14,* 47–53.

Luu, P., Tucker, D. M., Englander, R., Lockfeld, A., Lutsep, H., & Oken, B. (2001). Localizing acute stroke-related EEG changes: assessing the effects of spatial undersampling. *Journal of Clinical Neurophysiology, 18,* 302–317.

Makeig, S., Bell, A. J., Jung, T. P., & Sejnowski, T. J. (1996). Independent component analysis of electroencephalographic data. *Advances in Neural Information Processing Systems, 8,* 145–151.

Mann, E. O. & Paulsen, O. (2005). Mechanisms underlying gamma ('40 Hz') network oscillations in the hippocampus – a mini-review. *Progress in Biophysics and Molecular Biology, 87,* 67–76.

Maurer, K. & Dierks, T. (1991). *Atlas of Brain Mapping: Topographic Mapping of EEG and Evoked Potentials.* Berlin: Springer-Verlag.

Michel, C. M., Lehmann, D., Henggeler, B., & Brandeis, D. (1992). Localization of the sources of EEG delta, theta, alpha and beta frequency bands using the FFT dipole approximation. *Electroencephalography and Clinical Neurophysiology, 82,* 38–44.

Michel, C. M., Murray, M. M., Lantz, G., Gonzalez, S., Spinelli, L., & Grave, d. P. (2004). EEG source imaging. *Clinical Neurophysiology, 115,* 2195–2222.

Miller, C. E. & Henriquez, C. S. (1990). Finite element analysis of bioelectric phenomena. *Critical Reviews in Biomedical Engineering, 18,* 207–233.

Miltner, W. H., Braun, C., Arnold, M., Witte, H., & Taub, E. (1999). Coherence of gamma-band EEG activity as a basis for associative learning. *Nature, 397,* 434–436.

Moffitt, M. A. & Grill, W. M. (2004). Electrical localization of neural activity in the dorsal horn of the spinal cord: a modeling study. *Annals of Biomedical Engineering, 32,* 1694–1709.

Mosher, J. C. & Leahy, R. M. (1998). Recursive MUSIC: a framework for EEG and MEG source localization. *IEEE Transactions on Biomedical Engineering, 45,* 1342–1354.

Mosher, J. C., Lewis, P. S., & Leahy, R. M. (1992). Multiple dipole modeling and localization from spatio-temporal MEG data. *IEEE Transactions on Biomedical Engineering, 39,* 541–557.

Mulert, C., Gallinat, J., Pascual-Marqui, R., Dorn, H., Frick, K., Schlattmann, P. et al. (2001). Reduced event-related current density in the anterior cingulate cortex in schizophrenia. *Neuroimage, 13,* 589–600.

Mulert, C., Jager, L., Schmitt, R., Bussfeld, P., Pogarell, O., Moller, H. J. et al. (2004). Integration of fMRI and simultaneous EEG: Towards a comprehensive understanding of localization and time-course of brain activity in target detection. *Neuroimage, 22,* 83–94.

Murray, M. M., Michel, C. M., Grave, d. P., Ortigue, S., Brunet, D., Gonzalez, A. S. et al. (2004). Rapid discrimination of visual and multisensory memories revealed by electrical neuroimaging. *Neuroimage, 21,* 125–135.

Murthy, V. N. & Fetz, E. E. (1992). Coherent 25- to 35-Hz oscillations in the sensorimotor cortex of awake behaving monkeys. *Proceedings of the National Academy of Sciences of the United States of America, 89,* 5670–5674.

Niedermeyer, E. (1993). Historical Aspects. In E. Niedermeyer & F. Lopes da Silva (Eds.), *Electroencephalography: Basic principles, clinical applications, and related fields* (3rd ed., pp. 1–14). Baltimore: Williams & Wilkins.

Niedermeyer, E. (1993). Sleep and EEG. In E. Niedermeyer & F. Lopes da Silva (Eds.), *Electroencephalography: Basic Principles, Clinical Applications, and Related Fields* (3rd ed., pp. 153–166). Baltimore: Williams & Wilkins.

Nunez, P. L. & Pilgreen, K. L. (1991). The spline-Laplacian in clinical neurophysiology: a method to improve EEG spatial resolution. *Journal of Clinical Neurophysiology, 8,* 397–413.

Nunez, P. L. & Silberstein, R. B. (2000). On the relationship of synaptic activity to macroscopic measurements: does coregistration of EEG with fMRI make sense? *Brain Topography, 13,* 79–96.

Nunez, P. L., Srinivasan, R., Wijesinghe, R. S., Westdorp, A. F., Tucker, D. M., Silberstein, R. B., & Cadusch, P. J. (1997). EEG coherency. I: Statistics, reference electrode, volume conduction, Laplacians, cortical imaging, and interpretation at multiple scales. *Electroencephalography and Clinical Neurophysiology, 103,* 499–515.

Nuwer, M. R., Lehmann, D., Lopes da Silva, F., Matsuoka, S., Sutherling, W., & Vibert, J. F. (1999). IFCN guidelines for topographic and frequency analysis of EEGs and EPs. The International Federation of Clinical Neurophysiology. *Electroencephalography & Clinical Neurophysiology, 52 (Supplement),* 15–20.

Oakes, T. R., Pizzagalli, D. A., Hendrick, A. M., Horras, K. A., Larson, C. L., Abercrombie, H. C. et al. (2004). Functional coupling of simultaneous electrical and metabolic activity in the human brain. *Human Brain Mapping, 21,* 257–270.

Onton, J., Delorme, A., & Makeig, S. (2005). Frontal midline EEG dynamics during working memory. *NeuroImage, 27,* 341–356.

Oostenveld, R. & Praamstra, P. (2001). The five percent electrode system for high-resolution EEG and ERP measurements. *Clinical Neurophysiology, 112,* 713–719.

Pascual-Marqui, R. D. (1999). Review of methods for solving the EEG inverse problem. *International Journal of Bioelectromagnetism, 1,* 75–86.

Pascual-Marqui, R. D. (2002). Standardized low-resolution brain electromagnetic tomography (sLORETA): technical details. *Methods and Findings in Experimental and Clinical Pharmacology, 24 (Supplement D),* 5–12.

Pascual-Marqui, R. D., Esslen, M., Kochi, K., & Lehmann, D. (2002). Functional imaging with low-resolution brain electromagnetic tomography (LORETA): a review. *Methods and Findings in Experimental and Clinical Pharmacology, 24 (Supplement C),* 91–95.

Pascual-Marqui, R. D., Lehmann, D., Koenig, T., Kochi, K., Merlo, M. C., Hell, D. et al. (1999). Low resolution brain electromagnetic tomography (LORETA) functional imaging in acute, neuroleptic-naive, first-episode, productive schizophrenia. *Psychiatry Research: Neuroimaging, 90,* 169–179.

Pascual-Marqui, R. D., Michel, C. M., & Lehmann, D. (1994). Low resolution electromagnetic tomography: a new method for localizing electrical activity in the brain. *International Journal of Psychophysiology, 18,* 49–65.

Perrin, F., Bertrand, O., & Pernier, J. (1987). Scalp current density mapping: value and estimation from potential data. *IEEE Transactions on Biomedical Engineering, 34,* 283–288.

Perrin, F., Pernier, J., Bertrand, D., & Echallier, J. F. (1989). Spherical splines for scalp potential and current density mapping. *Electroencephalography & Clinical Neurophysiology, 72,* 184–187.

Pfurtscheller, G., Stancak, A., Jr., & Neuper, C. (1996). Event-related synchronization (ERS) in the alpha band – an electrophysiological correlate of cortical idling: A review. *International Journal of Psychophysiology, 24,* 39–46.

Phillips, C., Rugg, M. D., & Friston, K. J. (2002a). Anatomically informed basis functions for EEG source localization: Combining functional and anatomical constraints. *Neuroimage, 16,* 678–695.

Phillips, C., Rugg, M. D., & Friston, K. J. (2002b). Systematic regularization of linear inverse solutions of the EEG source localization problem. *Neuroimage, 17,* 287–301.

Pivik, R. T., Broughton, R. J., Coppola, R., Davidson, R. J., Fox, N., & Nuwer, M. R. (1993). Guidelines for the recording and quantitative analysis of electroencephalographic activity in research contexts. *Psychophysiology, 30,* 547–558.

Pizzagalli, D. A., Lehmann, D., Hendrick, A. M., Regard, M., Pascual-Marqui, R. D., & Davidson, R. J. (2002). Affective judgments of faces modulate early activity (approximately 160 ms) within the fusiform gyri. *Neuroimage, 16,* 663–677.

Pizzagalli, D. A., Nitschke, J. B., Oakes, T. R., Hendrick, A. M., Horras, K. A., Larson, C. L. et al. (2002). Brain electrical tomography in depression: The importance of symptom severity, anxiety and melancholic features. *Biological Psychiatry, 52,* 73–85.

Pizzagalli, D. A., Oakes, T. R., & Davidson, R. J. (2003). Coupling of theta activity and glucose metabolism in the human rostral anterior cingulate cortex: An EEG/PET study of normal and depressed subjects. *Psychophysiology, 40,* 939–949.

Pizzagalli, D. A., Oakes, T. R., Fox, A. S., Chung, M. K., Larson, C. L., Abercrombie, H. C. et al. (2004). Functional but not structural subgenual prefrontal cortex abnormalities in melancholia. *Molecular Psychiatry, 9,* 393–405.

Pizzagalli, D. A., Pascual-Marqui, R. D., Nitschke, J. B., Oakes, T. R., Larson, C. L., Abercrombie, H. C. et al. (2001). Anterior cingulate activity as a predictor of degree of treatment response in major depression: Evidence from brain electrical tomography analysis. *American Journal of Psychiatry, 158,* 405–415.

Pizzagalli, D. A., Peccoralo, L. A., Davidson, R. J., & Cohen, J. D. (2006). Resting anterior cingulate activity and abnormal responses to errors in subjects with elevated depressive symptoms: A 128-channel EEG study. *Human Brain Mapping, 27,* 185–201.

Pizzagalli, D. A., Sherwood, R. J., Henriques, J. B., & Davidson, R. J. (2005). Frontal brain asymmetry and reward responsiveness: A Source-localization study. *Psychological Science, 16,* 805–813.

Reddy, R. V., Moorthy, S. S., Mattice, T., Dierdorf, S. F., & Deitch, R. D., Jr. (1992). An electroencephalographic comparison of effects of propofol and methohexital. *Electroencephalography & Clinical Neurophysiology, 83,* 162–168.

Rodriguez, E., Lachaux, G. N., Martinerie, J., Renault, B., & Varela, F. L. (1999). Perception's shadow: Long distance synchronization of human brain activity. *Nature, 397,* 430–433.

Russell, G. S., Jeffrey, E. K., Poolman, P., Luu, P., & Tucker, D. M. (2005). Geodesic photogrammetry for localizing sensor

positions in dense-array EEG. *Clinical Neurophysiology, 116,* 1130–1140.

Samar, V. J., Bopardikar, A., Rao, R., & Swartz, K. (1999). Wavelet analysis of neuroelectric waveforms: A conceptual tutorial. *Brain and Language, 66,* 7–60.

Schack, B., Vath, N., Petsche, H., Geissler, H. G., & Moller, E. (2002). Phase-coupling of theta-gamma EEG rhythms during short-term memory processing. *International Journal of Psychophysiology, 44,* 143–163.

Schacter, D. L. (1977). EEG theta waves and psychological phenomena: A review and analysis. *Biological Psychology, 5,* 47–82.

Scherg, M. & Ebersole, J. S. (1994). Brain source imaging of focal and multifocal epileptiform EEG activity. *Neurophysiologie clinique, 24,* 51–60.

Schnitzler, A. & Gross, J. (2005). Normal and pathological oscillatory communication in the brain. *Nature Reviews Neuroscience, 6,* 285–296.

Seeck, M., Lazeyras, F., Michel, C. M., Blanke, O., Gericke, C. A., Ives, J. et al. (1998). Non-invasive epileptic focus localization using EEG-triggered functional MRI and electromagnetic tomography. *Electroencephalography & Clinical Neurophysiology, 106,* 508–512.

Soufflet, L., Toussaint, M., Luthringer, R., Gresser, J., Minot, R., & Macher, J. P. (1991). A statistical evaluation of the main interpolation methods applied to 3-dimensional EEG mapping. *Electroencephalography & Clinical Neurophysiology, 79,* 393–402.

Speckmann, E., Elger, C. E., & Altrup, U. (1993). Neurophysiologic basis of the EEG. In E. Wyllie (Ed.), *The Treatment of Epilepsy: Principles and Practices* (pp. 185–201). Philadelphia: Lea & Febiger.

Srinivasan, R., Tucker, D. M., & Murias, M. (1998). Estimating the spatial Nyquist of the human EEG. *Behavioral Research Methods, Instruments & Computers, 30,* 8–19.

Steriade, M. (1993). Cellular substrates of brain rhythms. In E. Niedermeyer & F. Lopes da Silva (Eds.), *Electroencephalography: Basic Principles, Clinical Applications, and Related Fields* (3rd ed., pp. 27–62). Baltimore: Williams & Wilkins.

Strik, W. K., Chiaramonti, R., Muscas, G. C., Paganini, M., Mueller, T. J., Fallgatter, A. J. et al. (1997). Decreased EEG microstate duration and anteriorisation of the brain electrical fields in mild and moderate dementia of the Alzheimer type. *Psychiatry Research, 75,* 183–191.

Sutton, S. K., & Davidson, R. J. (2000). Resting anterior brain activity predicts the evaluation of. affective stimuli. *Neuropsychologia, 38,* 1723–1733.

Szelies, B., Mielke, R., Kessler, J., & Heiss, W. D. (1999). EEG power changes are related to regional cerebral glucose metabolism in vascular dementia. *Clinical Neurophysiology, 110,* 615–620.

Tassinary, L. G., & Cacioppo, J. T. (2000). The skeletomuscular system: Surface electromyography. In J. T. Cacioppo, L. G. Tassinary, & G. G. Berntson (Eds.), *Handbook of psychophysiology*, 2nd edition (pp. 163–199). New York: Cambridge University Press.

Thakor, N. V. & Tong, S. (2004). Advances in quantitative electroencephalogram analysis methods. *Annual Review of Biomedical Engineering, 6,* 453–495.

Thatcher, R. W., Krause, P. J., & Hrybyk, M. (1986). Cortico-cortical associations and EEG coherence: A two-compartmental model. *Electroencephalography & Clinical Neurophysiology, 64,* 123–143.

Thut, G., Hauert, C. A., Morand, S., Seeck, M., Landis, T., & Michel, C. (1999). Evidence for interhemispheric motor-level transfer in a simple reaction time task: an EEG study. *Experimental Brain Research, 128,* 256–261.

Towle, V. L., Bolanos, J., Suarez, D., Tan, K., Grzeszczuk, R., Levin, D. N. et al. (1993). The spatial location of EEG electrodes: locating the best-fitting sphere relative to cortical anatomy. *Electroencephalography & Clinical Neurophysiology, 86,* 1–6.

Towle, V. L., Syed, I., Berger, C., Grzeszczuk, R., Milton, J., Erickson, R. K. et al. (1998). Identification of the sensory/motor area and pathologic regions using ECoG coherence. *Electroencephalography & Clinical Neurophysiology, 106,* 30–39.

Trujillo-Barreto, N. J., Aubert-Vazquez, E., & Valdes-Sosa, P. A. (2004). Bayesian model averaging in EEG/MEG imaging. *Neuroimage, 21,* 1300–1319.

Tsuno, N., Shigeta, M., Hyoki, K., Kinoshita, T., Ushijima, S., Faber, P. L. et al. (2002). Spatial organization of EEG activity from alertness to sleep stage 2 in old and younger subjects. *Journal of Sleep Research, 11,* 43–51.

Tuch, D. S., Wedeen, V. J., Dale, A. M., George, J. S., & Belliveau, J. W. (1999). Conductivity mapping of biological tissue using diffusion MRI. *Annals of the New York Academy of Sciences, 888,* 314–316.

Tucker, D. M. (1993). Spatial sampling of head electrical fields: The geodesic sensor net. *Electroencephalography & Clinical Neurophysiology, 87,* 154–163.

Uchida, S., Nakayama, H., Maehara, T., Hirai, N., Arakaki, H., Nakamura, M. et al. (2000). Suppression of gamma activity in the human medial temporal lobe by sevoflurane anesthesia. *Neuroreport, 11,* 39–42.

Valdes-Sosa, P., Marti, F., Garcia, F., and Casanova, R. (1996). Variable Resolution Electric-Magnetic Tomography. In C. Wood (Ed.), *Proceedings of the Tenth International Conference on Biomagnetism*. Santa Fe, New Mexico.

Vertes, R. P. & Kocsis, B. (1997). Brainstem-diencephalo-septohippocampal systems controlling the theta rhythm of the hippocampus. *Neuroscience, 81,* 893–926.

Vinogradova, O. S. (1995). Expression, control, and probable functional significance of the neuronal theta-rhythm. *Progress in Neurobiology, 45,* 523–583.

Vitacco, D., Brandeis, D., Pascual-Marqui, R., & Martin, E. (2002). Correspondence of event-related potential tomography and functional magnetic resonance imaging during language processing. *Human Brain Mapping, 17,* 4–12.

von Stein, A. & Sarnthein, J. (2000). Different frequencies for different scales of cortical integration: from local gamma to long range alpha/theta synchronization. *International Journal of Psychophysiology, 38,* 301–313.

Wagner, M., Fuchs, M., & Kastner, J. (2004). Evaluation of sLORETA in the presence of noise and multiple sources. *Brain Topography, 16,* 277–280.

Weiss, S. & Mueller, H. M. (2003). The contribution of EEG coherence to the investigation of language. *Brain and Language, 85,* 325–343.

Worrell, G. A., Lagerlund, T. D., Sharbrough, F. W., Brinkmann, B. H., Busacker, N. E., Cicora, K. M. et al. (2000). Localization of the epileptic focus by low-resolution electromagnetic tomography in patients with a lesion demonstrated by MRI. *Brain Topography, 12,* 273–282.

Yao, J. & Dewald, J. P. (2005). Evaluation of different cortical source localization methods using simulated and experimental EEG data. *Neuroimage, 25,* 369–382.